

MAISE: Construction of neural network interatomic models and evolutionary structure optimization

Samad Hajinazar^a, Aidan Thorn^a, Ernesto D. Sandoval^a, Saba Kharabadze^a, and Aleksey N. Kolmogorov^{a,*}

^a*Department of Physics, Applied Physics and Astronomy, Binghamton University, State University of New York, PO Box 6000, Binghamton, New York 13902-6000, United States*

^{*}*Corresponding author: kolmogorov@binghamton.edu*

Abstract

MAISE is an open-source package for materials modeling and prediction. The code's main feature is an automated generation of neural network (NN) interatomic potentials for use in global structure searches. The systematic construction of Behler-Parrinello-type NN models approximating *ab initio* energy and forces relies on two approaches introduced in our recent studies. An evolutionary sampling scheme for generating reference structures improves the NNs' mapping of regions visited in unconstrained searches, while a stratified training approach enables the creation of standardized NN models for multiple elements. A more flexible NN architecture proposed here expands the applicability of the stratified scheme for an arbitrary number of elements. The full workflow in the NN development is managed with a customizable 'MAISE-NET' wrapper written in Python. The global structure optimization capability in MAISE is based on an evolutionary algorithm applicable for nanoparticles, films, and bulk crystals. A multitribe extension of the algorithm allows for an efficient simultaneous optimization of nanoparticles in a given size range. Implemented structure analysis functions include fingerprinting with radial distribution functions and finding space groups with the SPGLIB tool. This work overviews MAISE's available features, constructed models, and confirmed predictions.

1 Introduction

Module for *ab initio* structure evolution (MAISE) was first written as a standalone C code in 2009 [1]. It was originally designed as an evolutionary optimization engine interfaced with external density functional theory (DFT) packages to enable unconstrained ground state structure searches. The implemented evolutionary algorithm followed a general principle of using natural selection to evolve populations of structures with crossover and mutation operations [2, 3, 4, 5, 6, 7, 8, 9, 10, 11, 12, 13, 14, 15, 16]. MAISE-specific features include radial distribution function (RDF)-based structure fingerprinting for detecting and eliminating similar population members [1, 17, 18] and an efficient co-evolutionary optimization of nanoparticles (NP) in a given size range via sharing of best motifs among multiple tribes [19, 20]. *Ab initio* predictions made with MAISE and confirmed in experimental studies are overviewed in Section 2.

The primary function of the present MAISE package is the construction of NN interatomic models for accurate mapping of *ab initio* potential energy surfaces. The significant advances in the application of machine learning methodology to the description of interatomic interactions [21, 22, 23, 24, 25, 26, 27, 28, 29, 30, 31, 32, 33, 34, 35, 36, 37, 38, 39, 40, 41, 42, 43, 44, 19, 20, 45, 46, 47, 48, 49, 50, 51, 52, 53, 54] opened up the possibility of accelerating *ab initio* structure

prediction. Our examinations of NN performance in prediction of stable compounds have revealed limitations of the traditional approaches used to sample configuration spaces and train NNs for multiple elements [34]. An evolutionary sampling and a stratified training schemes introduced in Ref. [34] and discussed in Section 8 have allowed us to build reliable NN models for extended sets of metals. Our developed MAISE-NET Python script streamlines all stages of the process, from generating reference structures and handling external *ab initio* calculations to performing NN training and testing. With the machine learning module and relevant utility functions comprising about 9,130 out of 14,364 lines of the full code, a more descriptive reading of the MAISE acronym at this point is 'module for artificial intelligence and structure evolution'.

MAISE can perform local/global optimizations, molecular dynamics (MD), and basic phonon calculations by evaluating the total energy, atomic forces, and unit cell stresses for given structures at the NN or empirical potential levels. The main input/output files have a general VASP [55, 56] format to simplify interfacing MAISE with other structure prediction and property analysis engines (PyChemia [57], PHON [58], etc.). The NN training and structure simulation modules are parallelized with OpenMP [59]. Command-line structure analysis and manipulation operations, such as structure comparison or space group determination, are listed in Section 4.

2 Confirmed predictions

The reliability of *ab initio* predictions for finding new materials depends on the accuracy of the theoretical method for computing the structure stability (Gibbs free energy) and the exhaustive sampling of large configuration spaces (structures and compositions). A common approach to evaluating Gibbs free energy with continually improving DFT approximations [60, 61, 62, 63, 64, 65, 66] is to determine the enthalpy at $T = 0$ K and then include the temperature-dependent vibrational/configurational entropy terms for viable candidates. Explorations of configurational spaces can be done with a variety of advanced structure prediction methods introduced in the past two decades [7, 8, 67, 68, 69, 70, 71, 72, 73, 74, 75, 76, 77, 78, 79]. The search strategy employed in our predictive work has involved (i) high-throughput (HT) screening of known relevant prototypes to establish a baseline for compound stability; (ii) unconstrained evolutionary search (ES) to identify new stable motifs; and (iii) stability analysis to explain or improve the stability of identified materials.

Here, we recount notable factors leading to successful predictions and provide context on the discovered materials' significance (Figure 1 and Table 1). In terms of novelty, (i) FeB_4 [1, 80, 81], LiB [82, 83, 84], and NaSn_2 [85, 86] are new phases predicted before their experimental realization; (ii) CaB_6 [17] and $\text{Na}_3\text{Ir}_3\text{O}_8$ [87] are solutions of complex phases synthesized and characterized in joint studies; and (iii) Na_2IrO_3 [88], CrB_4 [80, 89], and MnB_4 [90, 91, 92] are confirmed revisions of previously misidentified crystal structures. All cases except for Na_2IrO_3 involved extensive evolutionary searches and resulted in brand-new crystal structures for FeB_4 , CrB_4 , MnB_4 , CaB_6 , and $\text{Na}_3\text{Ir}_3\text{O}_8$. All phases except for $\text{Na}_3\text{Ir}_3\text{O}_8$ have been either synthesized at or successfully quenched down to the ambient pressure.

FeB_4 [1, 80, 81] is an early example of a superconductor predicted fully '*in silico*'. With a combination of HT screening, ESs, and electron-phonon calculations, we demonstrated that an FeB_4 compound should become thermodynamically stable under moderate pressures around 10 GPa in a brand-new oP10 crystal structure (SG#58), remain metastable under normal conditions, and exhibit phonon-mediated superconductivity unusual for an Fe-containing material. The subsequent discovery of the superconductor [81] has motivated further studies [93, 94].

LiB was proposed to be a new synthesizable layered phase [82, 83] with electronic features

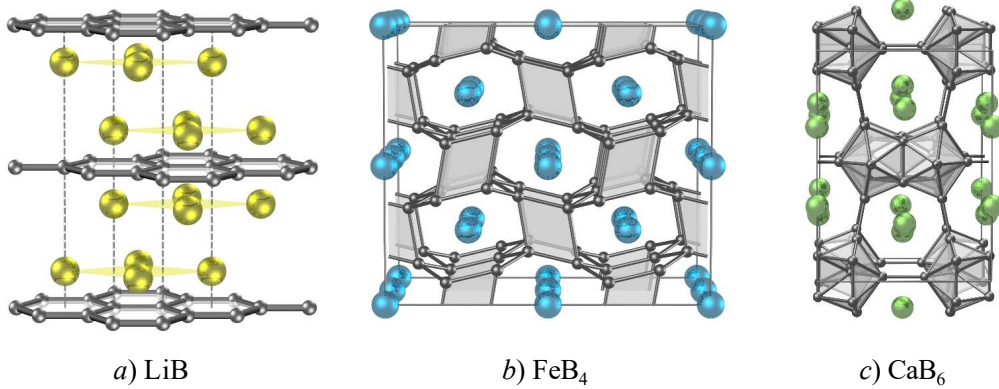


Figure 1: Structures of select MAISE confirmed predictions detailed in Table 1. The small (large) spheres show boron (metal) atoms.

desirable for MgB_2 -type superconductivity [95]. The set of 'metal sandwich' configurations was constructed by analyzing stability trends in our HT data. In order to determine suitable synthesis conditions, we explained the off-stoichiometric LiB_x material and modeled the complex behavior of the two competing phases under high pressures. Our synthesis and XRD analysis confirmed the predicted shifts in the LiB_x composition and the existence of the LiB phase with random stacking [84]. The demonstration of the LiB metastability under ambient pressure should simplify future study of the material's superconductivity.

NaSn_2 [85] was predicted to be an overlooked phase synthesizable under ambient pressure. With the primary focus on finding new bulk Sn materials that could be exfoliated into stanene, we examined a set of layered Sn alloys and showed that Na stabilizes a rigid 3D framework with flat Sn layers. Our electronic structure analysis indicated that the compound should have non-trivial topological properties. The predicted hP3- NaSn_2 phase (SG#191) was observed later in an independent experiment [86].

CaB_6 proved to be the most challenging case in our structure prediction work. A preliminary ground state search uncovered several CaB_6 polymorphs stabilized by high pressure but none of them matched the high-pressure XRD patterns obtained in our concurrent experiments [17]. An ES for a larger 28-atom unit cell eventually converged to a new tI56 structure (SG#139) with unique boron building blocks that explained the convoluted XRD data. In contrast to studies that determined ground states of similar size, the ES for CaB_6 did not use any structural input from experiment, which makes tI56 one of the largest confirmed crystal structures found truly 'from scratch'. Our follow-up tests for tI56- CaB_6 , oC88-Li, and γ - B_{28} showed that the use of unit cell dimensions extracted from XRD makes it possible to find the ground state one-two orders of magnitude faster [17].

$\text{Na}_3\text{Ir}_3\text{O}_8$ was experimentally observed to transform into a lower-symmetry phase under pressure. Given the considerable size of the 56-atom ambient-pressure ground state, we used it to initialize our ES but did not rely on any high- P experimental data. An independently obtained mP56 solution (SG#4) with a dimerized Ir-Ir network turned out to be in excellent agreement with the collected XRD patterns [87].

phase structure	prediction confirmation	synthesis P quenched P	properties remarks
FeB ₄ oP10	2010 [1, 80] 2013 [81]	10 GPa 1 bar	Fe-based BCS superconductor predicted fully 'from scratch'
LiB hP4-8	2006 [82, 83] 2015 [84]	21 GPa 1 bar	proposed MgB ₂ -type superconductor cold compression synthesis
NaSn ₂ hP3 (AlB ₂)	2016 [85] 2017 [86]	1 bar	3D Sn framework with flat Sn layers non-trivial topological properties
CaB ₆ tI56	2012 [17] 2012 [17]	31 GPa 1 bar	unique boron building blocks found w/o any structural input
Na ₃ Ir ₃ O ₈ mP56	2018 [87] 2018 [87]	11 GPa 1 bar	dimerized Ir framework found w/o any high-P structural input
Na ₂ IrO ₃ mS24	2012 [88] 2012 [88]	1 bar	candidate for the Kitaev model revised structure
CrB ₄ oP10	2011 [80] 2012 [89]	1 bar	distorted 3D boron framework misidentified for over 40 years
MnB ₄ mP20	2014 [90] 2014 [91, 92]	1 bar	distorted 3D boron framework unsolved for over 40 years

Table 1: MAISE confirmed predictions with listed ground state structures, synthesis pressure, established metastability under normal conditions (for phases synthesized at high pressures), key features, and general observations.

Na₂IrO₃ structure was originally assigned SG#15 (*C*2/*c*) [96]. A simple local optimization revealed the ground state to have SG#12 (*C*2/*m*) in agreement with the experimental solution established by our colleagues in a joint study [88]. Our RDF analysis helped rationalize the bond rearrangement resulting in the more stable configuration. The compound has received considerable attention as a candidate for the realization of the Kitaev model.

CrB₄ [80] was first synthesized over 50 years ago and represented as an oI10 structure (SG#71). Having determined that FeB₄ is significantly more stable in the related distorted oP10 configuration (SG#58) [1, 80], we re-examined CrB₄ and showed oP10 to be the ground state for this compound as well. The significant distortion of the 3D boron framework was shown to have little effect on the powder XRD patterns which explained the mischaracterization of the CrB₄ structure. Following electron diffraction [89] and single-crystal XRD [97] measurements confirmed the revised oP10 solution for CrB₄.

MnB₄ [90] was also synthesized over 50 years ago and tentatively assigned an mS10 (SG#12) structure. Our ES found a more stable mP20 (SG#14) derivative in early 2013. Matching solutions were obtained independently by several groups around the same time [91, 92].

Our predictive work has shown that crystalline ground states can be found rather routinely without the need of advanced structure prediction algorithms if (i) the unit cells have fewer than

about 10 atoms; (ii) the search is initialized with related configurations; or (iii) the search is constrained with unit cell dimensions extracted from experiment. The ES becomes essential for larger systems, especially when no prior information is available.

3 Installation

Download The full MAISE package, currently MAISE version 2.5 and MAISE-NET version 1.0, can be obtained from the Github repository [98, 99]. It contains MAISE C-language source code, MAISE-NET Python script (Section 8), available NN and empirical potential models (Section 9), and basic examples.

Compilation The source code for MAISE can be compiled with: `$ make --jobs`. During MAISE compilation, the makefile script checks if two required external libraries, GSL [100] and SPGLIB (v1.11.2.1, Feb 2019) [101], are present. If not, they will be automatically downloaded to `./ext-dep` and installed in `./lib` on most systems. If the GSL or SPGLIB installation is not completed automatically the user should compile them manually and copy (i) `libgsl.a`, `libgslcblas.a` and `libsymspg.a` into the `'./lib'` subdirectory; (ii) the `'spglib.h'` header into `'./lib/include'` subdirectory; and (iii) all `gsl` headers into the `'./lib/include/gsl'` subdirectory.

Post-compilation test A `'check'` script is available in the `'./examples/'` directory which can be run after compiling the MAISE executable to ensure the proper function of the code. The script parses a small dataset, trains a basic NN, and optimizes a crystal structure. Error logs are generated in case any issues are detected.

4 Unit cell analysis and manipulation

A variety of structure analysis and manipulation tools are implemented in MAISE package which can be used in the command-line with the corresponding task-specifier flag. Working primarily with the VASP structure format (POSCAR file) as input, MAISE can determine the space group, calculate the radial distribution function (RDF) [1, 17], measure the similarity of two structures via RDF pattern comparison, calculate volume per atom for bulk and cluster geometries [102], align the cluster in the simulation box along the high symmetry axes, etc. The code expects a 'POSCAR' file in the running directory for operations involving a single structure or two 'POSCAR0' and 'POSCAR1' files for structure comparison. The tasks listed in Table 2 can be performed in the command line by running: `$ maise -[flag]`.

The similarity, or dot product, between two structures $k = 1, 2$ with species N_{spc} has been defined in MAISE as

$$C_1 \cdot C_2 = \sum_n \sum_{s1} \sum_{s2} \text{RDF}_{1,s1,s2}(R_n) \text{RDF}_{2,s1,s2}(R_n) / (\text{norm}_1 \text{norm}_2),$$

$$\text{norm}_k = \left[\sum_n \sum_{s1} \sum_{s2} \text{RDF}_{1,s1,s2}(R_n) \text{RDF}_{2,s1,s2}(R_n) \right]^{1/2}.$$

The RDFs are defined for each structure k at each bin $R_n = n/N_{\text{bin}} R_{\text{hard}}$ ($N_{\text{bin}} = 3,000$) as

$$\text{RDF}_{k,s1,s2}(R_n) = \sum_{i, si=s1}^{N_{\text{atom}}} \sum_{j, sj=s2}^{N_{\text{atom}}} e^{-\frac{(R_{ij} - R_n)^2}{2\sigma^2}} f_{\text{cut}}(R_n),$$

where si and sj denote the species of atoms i and j , respectively. $f_{\text{cut}}(R_n) = 1$ for $R_n < R_{\text{soft}}$ and $f_{\text{cut}}(R_n) = \cos\left(\pi/2 \frac{R_n - R_{\text{soft}}}{R_{\text{hard}} - R_{\text{soft}}}\right)$ for $R_{\text{soft}} < R_n < R_{\text{hard}}$. For efficiency purposes, only $R_n - 3\sigma < R_{ij} < R_n + 3\sigma$ are included in the sum.

The dot product is sensitive to the choice of R_{soft} , R_{hard} , and σ . It is good practice to include at least two shells of nearest neighbors ($R_{\text{hard}} \gtrsim 5 \text{ \AA}$) and use sharper Gaussians ($\sigma \approx 0.008 \text{ \AA}$) for disordered or cluster structures and wider ones for high-symmetry structures ($\sigma \approx 0.02 \text{ \AA}$).

flag	description
man	output the list of available flags
rdf	compute the RDF for POSCAR
cxc	compute dot product for POSCAR0 and POSCAR1 using RDF
cmp	compare RDF, space group, and volume of POSCAR0 and POSCAR1
spg	convert POSCAR into str.cif, CONV, PRIM
cif	convert str.cif into CONV
rot	rotate a cluster along eigenvectors of moments of inertia
dim	find whether POSCAR is periodic (3) or non-periodic (0)
box	reset the box size for clusters
sup	make a $N_a \times N_b \times N_c$ supercell
vol	compute volume per atom for crystals or clusters

Table 2: List of the available command-line flags in MAISE package for structure analysis and manipulation.

5 Structure simulation

Available structure simulation functions include unit cell relaxation, MD, and phonon property analysis. The structure, the interaction model, and the job settings are specified in 'POSCAR', 'model', and 'setup' files, respectively.

5.1 Local structure optimization

Structure optimization with analytic derivative-based BFGS [103] or CG [104] algorithms can be performed by using NN or other classical interatomic interaction models available in MAISE. The local optimization is carried out until the maximum number of iterations (MITR) or the targeted enthalpy difference between successive steps (ETOL) is reached. The full list of relevant 'setup' parameters for the local optimization task is provided in Table A3.

The unit cell parameters, total/atomic energies, and force/stress components can be outputted at each relaxation step in an 'OUTCAR' file, while the final structure is saved in a 'CONTCAR' file. This information saved in the VASP-style format can be utilized by external codes to perform vibrational property analysis, global structure optimization, etc.

5.2 Molecular dynamics simulations

MD simulations can be run in the microcanonical ensemble (NVE) with the Verlet algorithm [105], the canonical ensemble (NVT) with the Nosé-Hoover thermostat [106, 107], and isobaric-isothermal ensemble (NPT) with a combination of the Nosé-Hoover thermostat and the Berendsen barostat [108]. The velocities are initialized either according to the Maxwell distribution at a given

starting temperature or with the values specified in the 'POSCAR' file. Table A4 lists 'setup' parameters relevant for MD simulations. MAISE outputs energies, lattice parameters, Lindemann index, average RDF, etc. for each temperature. In the current version of MAISE, Lindemann index value is well-defined only for NPs and the barostat is implemented for unit cells with orthogonal lattice vectors.

Figure 2 illustrates the use of the *NPT* ensemble and our latest NN model for evaluating the linear thermal expansion coefficient $\alpha = \frac{1}{L} \left(\frac{\partial L}{\partial T} \right)_P$ in Ag near room temperature. A 108-atom $3 \times 3 \times 3$ supercell of FCC-Ag was simulated at $T = 300 \pm 10$ K for 0.5 ns with a 1 fs time step (500,000 integration steps in total) to find the numerical temperature derivative of the lattice constants. Allowing the first 0.025 ns for equilibration, we observed convergence of α to within 0.5% in the following 0.25 ns. Simulations of FCC-Cu and BCC-Na showed similar convergence rates. The resulting linear thermal expansion coefficients of 21.0×10^{-6} K $^{-1}$ for Ag, 14.9×10^{-6} K $^{-1}$ for Cu, and 51.7×10^{-6} K $^{-1}$ for Na are within 10-30% relative to the corresponding experimental values of 19.0×10^{-6} K $^{-1}$, 16.7×10^{-6} K $^{-1}$, and 69×10^{-6} K $^{-1}$ [109]. Simulations with a smaller temperature difference $T = 300 \pm 5$ K and a larger structure (256-atom $4 \times 4 \times 4$ supercell of FCC-Ag) showed similar results for the expansion coefficient.

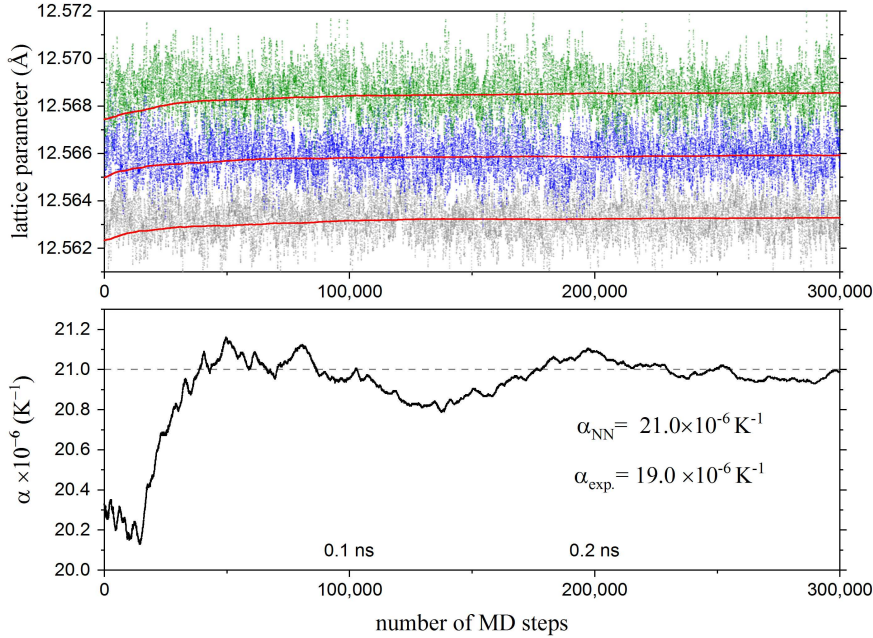


Figure 2: (Top panel) Fluctuations of the lattice parameter for a 108-atom supercell of FCC-Ag at $T = 290$ K (grey), $T = 300$ K (blue), and $T = 310$ K (green) along with the corresponding average lattice parameters (red) as a function of the number of MD steps. (Bottom panel) Linear thermal expansion coefficient (α) at $T = 300$ K as a function of the number of MD steps. The calculated linear expansion coefficient for Ag is in 10% agreement with the measured value [109].

5.3 Phonon calculations

Our studies of vibrational properties [20] have been performed with an external PHON package [58] because it readily links with VASP or MAISE for a consistent comparison of the NN models against the DFT. Presently, MAISE has an internal option to calculate Γ -point phonons with the frozen phonon method in the quasi-harmonic approximation. The dynamical matrix is constructed

by numerical differentiation of the atomic forces. The magnitude of atomic displacements of each atom is defined by the 'DISP' parameter. Due to the negligible numerical noise of the NN analytic forces, the displacement values can be kept small to reduce the anharmonic effects and satisfy the acoustic sum rule (a list of setup parameters for phonon calculations in MAISE code is presented in Table A5).

The main application of this basic feature is to determine the presence of soft frequencies in the analysis of structures' dynamical stability. The code marks trivial zero-frequency translational (and rotational) modes by checking whether the eigenvectors generate net linear (and angular) momenta in crystals (and clusters). Ordered frequencies and the corresponding eigenvectors are printed in the 'OUTCAR' file and can be used for introducing soft-mode mutations in global evolutionary searches [110] or monitoring nudged elastic band method convergence in transition state searches.

6 Evolutionary search

Overview Evolutionary algorithms rely on Nature's heredity and 'survival of the fittest' principles for optimizing complex systems. MAISE enables the search for lowest-enthalpy bulk crystals, flat films, or NPs at a fixed chemical composition. The majority of the algorithm's numerous internal parameters related to the generation, evolution, and selection of structures have been tuned for typical crystalline unit cells with up to about 50 atoms and NPs with a few hundred atoms. Below we briefly overview the key settings adjustable by the user for the algorithm's optimal performance.

Interaction description method The evolutionary optimization module expects local relaxations of structures to be performed by an external code (flag CODE) through a queueing system (flag QUET). The current version is linked with VASP for DFT calculations and with MAISE for NN calculations. In case of fast Lennard-Jones, Gupta, or Sutton-Chen potentials, local optimization calls can be made directly from the evolutionary engine in MAISE. Input files and submission scripts for DFT/NN relaxations should be specified in the INI directory.

Population initialization Bulk ground state searches can be initialized via (i) randomization of given structures to bias the search toward nearby stable configurations; (ii) randomization of atoms in a constrained unit cell to make use of available information from XRD; and (iii) unbiased generation of random unit cells and atomic positions. In case the structures have interatomic distances shorter than a tabulated species- and pressure-dependent value, they are adjusted using a simple repulsive interatomic potential or re-generated. NPs can be created with a TETRIS-like function introduced in our recent study [19] that ensures good packing and customizable radial/angular distributions of species. 2D films are constrained to the x - y plane at the beginning and duration of the ES [111].

Evolution operations Offspring bulk structures are obtained with mutation or crossover operations. The former acts on a randomly chosen parent structure to distort lattice vectors, displace atomic positions, and/or swap atoms of different species. The latter randomly picks two parent structures, rotates the lattice vectors to ensure the best matching of unit cell dimensions, slices the unit cells approximately in half, and combines the pieces with small adjustments at the boundary to avoid short interatomic distances. Offspring NPs can also be created with alternative "Rubik's Cube" and "spherical cut crossover" operations, described in our previous study and used to quantify the effectiveness of the traditional crossover [19].

Structure selection Once a new generation is locally optimized, the joint population of parent and child structures is ranked according to their enthalpy and each structure n is assigned the survival probability proportional to $1/2(1-\tanh[2(H_n-H_{min})/(H_{max}-H_{min})-1])$ where H_{min} and H_{max} are lowest and highest enthalpies in the population, respectively [112]. Duplicate structures

determined to have similar RDFs, energies, and volumes are assigned zero chance of survival. Structures are eliminated one by one until the merged population is reduced to its original size. Ground states with 10-16 atoms per primitive unit cells are usually found in 1,000-3,000 local optimizations. Configurations with large lattice constant differences (e.g., long stacking sequences) and low atomic densities (e.g., the low-coordination diamond structure) tend to take longer to appear.

Job execution The evolutionary optimization is executed by running MAISE in the background. The search (re)starts from a given generation and proceeds for a specified number of iterations (flag NITR). In each cycle, the code generates a new population, submits a job for each structure to a specified queue, checks if the jobs finished successfully, processes the results, and outputs enthalpy/volume for each structure.

Multitribe optimization The efficient co-evolutionary simultaneous optimization of NPs introduced and tested in our recent study [20] requires a separate bash script. The wrapper manages the submission of ESs and the exchange of seeds among tribes at the end of each cycle of isolated evolution.

ES output The ES progress can be monitored by visualizing the enthalpy profile and heredity of population members saved in 'ebest.dat', 'erank.dat', and 'elink.dat' files (see Figure 3). The connections between points in consequent generations illustrate which parent structures were used to generate the offspring: one for mutations and two for crossovers. After an ES is completed, one can select distinct low-enthalpy structures in the entire pool of locally optimized members by running a post-search analysis with JOBT=13. Configurations with dissimilar RDF dot products by at most SCUT (e.g., 0.95) and with enthalpies at most DENE (e.g., 20 meV/atom) above the lowest-enthalpy structure will be saved and optionally relaxed at the DFT level.

ES example Figure 3 illustrates the performance of a typical ES. Structures with Mg_8Ca_4 unit cells were modeled with our latest NN interatomic potential. A population of 32 members was evolved for 40 generations and converged to the known C14 Laves phase ground state, producing the metastable C15 along the way. Our previous study revealed that C15/C36- Mg_2Ca and oS36/mS18- Mg_7Ca_2 could be overlooked phases synthesizable under high temperatures while B2- $MgCa$ and cF16- Mg_3Ca are thermodynamically stable under high pressures [40]. To the best of our knowledge, they are the first examples of new synthesizable compounds predicted with global structure searches based on NN interatomic potentials.

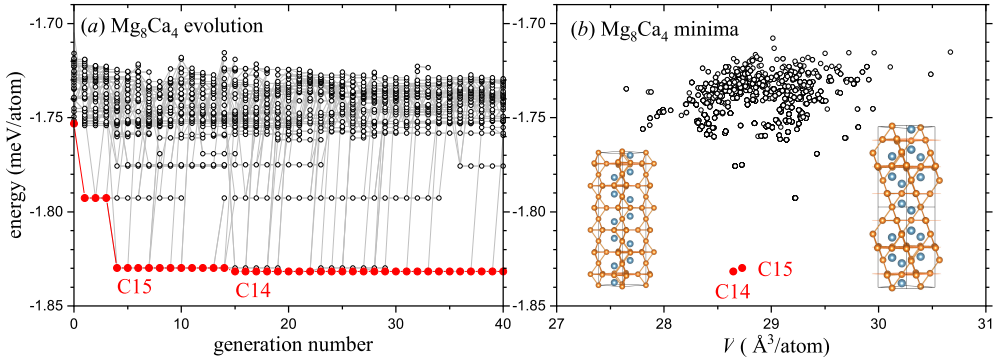


Figure 3: Typical results of ES runs performed with MAISE. This global structure search at the Mg_8Ca_4 composition identified both the metastable C15 Laves phase and the C14 ground state. The interactions were modeled with the latest Mg-Ca NN interatomic potential. (a) Energy distribution and structure heredity for an ES with 40 generations and 32 members in the population. (b) Collection of all local/global minima at the end of the ES.

7 Neural network model construction

In contrast to traditional classical potentials crafted to describe particular interaction types [113, 114, 115, 116, 117, 118, 119, 120, 121, 122], common NN models are intentionally kept devoid of any embedded physics to achieve better transferability [31]. The NNs' great interpolation power comes with users' great responsibility to generate proper reference datasets and perform careful fitting. This section describes key steps for building general NN interatomic potentials and overviews guidelines for constructing practical NNs applicable to compound prediction.

7.1 Reference data generation

The starting point in NN construction involves choosing a suitable reference interaction description method and selecting particular parts of the potential energy surface (PES) to approximate. Both choices are essential because NNs inherit the method's systematic/numerical errors and represent the PES well only in or near the sampled regions. While there are well-established comparable DFT approximations that can be picked to describe targeted materials properties [60, 61, 62, 63, 64, 65, 66], automated protocols for generating reference dataset are still being developed and tested [26, 34, 41, 123, 124, 125, 126, 127].

As a general principle, it is natural to expose NNs to typical configurations that will be encountered in intended applications, such as ground/transition state searches, MD, Monte-Carlo simulations, vibrational property calculations, etc. In our previous study dedicated to unconstrained searches [34], we departed from the popular MD-based scheme and introduced an evolutionary sampling approach reviewed and generalized further in Section 8. With the bulk of the diverse dataset created in an unsupervised fashion, we keep an option open for customized input.

One important recourse discussed in Ref. [34] is the incorporation of equation of state (EOS) data for select structures, e.g., the dimer, FCC, BCC, HCP, etc., which helps reduce the number of NN artifacts. We demonstrated [34] that inclusion of such structures with very short and very long interatomic distances has little effect on the NN description of low-energy structures but teaches the NN to disfavor unphysical configurations that can be inadvertently probed in global searches or MD runs. We found this approach to work better than the common introduction of a repulsive potential. Another beneficial option is the elimination of structures that are either too similar to each other or clearly irrelevant. The reduction of similar structures is performed naturally in our short evolutionary runs during data generation. The exclusion of structures with high energy or forces is done during data filtering as detailed in the next Section. Our typical datasets consist of 86% of evolutionary data with 1-8 atoms per unit cell, 12% of EOS data, and 2% of structures obtained during evolutionary testing of NN models (more details in Section 8).

Standard target values taken from DFT calculations are total energies, atomic forces, and unit cell stresses. In energy training, the outputs of an atomistic NN model need to be summed up for an entire unit cell before they can be compared against the corresponding DFT value. In energy-force training, implemented and examined in our studies in early 2000's [128], the dataset is expanded dramatically with more direct information about local environments. Due to the correlation of forces on nearby atoms according to Newton's 3rd law, we randomly pick only 25-50% of atoms with non-zero forces in a structure. The resulting ratios of force to energy data in our studies are at least 7:1.

7.2 Data filtering and parsing

The data processing step allows the user to filter out irrelevant configurations, earmark structures for training and testing, and parse atomic environments into NN inputs. These operations can be

customized by choosing flags in the 'setup' file, arranging the data by type into subdirectories, and specifying Behler-Parrinello (BP) symmetry functions [21] in the 'basis' file.

In data filtering, the ECUT, EMAX, and FMAX flags described in Table A8 control the maximum values of energy (enthalpy) and forces allowed in the database. A single energy cutoff is ill-defined or not helpful if the database contains entries with different structure types (clusters or crystal structures), compositions (in multielement systems), or simulation conditions (pressure values). Provided that the data is sorted in subdirectories by type, ECUT and EMAX are applied to the energy per atom within each subset. These values can be overwritten for a specific subset by placing a 'tag' file in the corresponding subdirectory. This 'tag' file can also be used to promote the inclusion of the subset, e.g., EOS data, into the training set.

The energy and force cutoff parameters are critical for striking a balance between the accuracy and the reliability of a NN. It may be tempting to keep EMAX and FMAX below about 0.5 meV/atom and 1 eV/Å, respectively, for exploration of (nearly) stable phases. However, our tests have shown that such NNs develop numerous artificial minima easily accessible in MD or structure optimization runs, a problem known not only for NNs but also for traditional potentials. We have found that when the cutoff values are raised to 5 eV/atom and 10 eV/Å, and even higher for EOS data, the NNs lose 1-2 meV/atom in accuracy but become robust enough to be used in unconstrained searches.

In data parsing, the idea is to precompute and store NN inputs for each structure only once to avoid performing this costly operation at each NN fitting step. The BP symmetry functions used for the conversion can be easily customized by adjusting the parameters in the 'basis' file. We typically use the set with 51 functions per element with the cutoff expanded from 6.0 Å to 7.5 Å and the corresponding η parameters rescaled by a factor of 1.25 (as described in our previous study [40]).

The filtering, earmarking, and parsing operations are done in a single JOBT=30 run. It produces a file for each structure with parsed energy/force NN inputs and collects statistics on the energy, force, volume, and RDF distributions in the full dataset.

7.3 Neural network training

The default NN implemented in MAISE has a standard feed-forward architecture with one bias per input or hidden layer. Signals are processed with hyperbolic activation functions in hidden layers and with the linear function in the output neuron. Our tests on metallic alloys have shown comparable performances of one- or two-layer NNs with the same total number of neurons and insignificant NN accuracy improvements beyond 20 neurons [34]. Based on these observations, we have adopted the 51-10-10-1 architecture with $(51+1) \times 10 + (10+1) \times 10 + (10+1) = 641$ adjustable parameters per chemical element.

The filtered and parsed data is split into training and testing sets with the NTRN and NTST flags, usually at the 9:1 ratio. Data earmarked for training with 'tag' files in the corresponding subdirectories (see Section 7.2) has a higher priority to be placed into the training set.

NN fitting via backpropagation can be performed with BFGS or CG algorithm as implemented in the GSL. Analytic derivatives of the weights are used in both energy and force training, with the latter procedure being slower by a factor of ~ 3 per data point. In order to balance the significance of the energy and force data, the contributions to the full error function from the mismatches between the NN and target force component values are multiplied by 0.1 Å (throughout the present work, 'error' represents the root-mean-square error). The NN weights are initialized randomly or read in from a previous 'model' file.

The optimization is usually carried out for $1 - 5 \times 10^5$ epochs. We have observed that initial

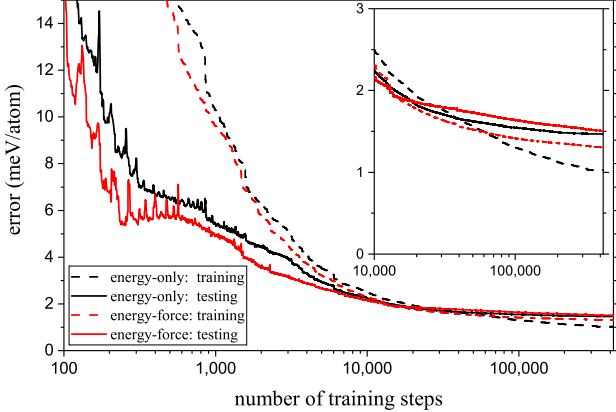


Figure 4: Error convergence in optimizations of a Cu-Ag NN model with 1,880 adjustable parameters for the same binary structure set with 5,352 energy-only training data (black lines) or 5,352-37,803 energy-force training data (red lines). The ratio of the training to testing data is 9:1. The training errors (dashed lines) are higher than the testing errors (solid lines) for the first 20,000 steps because the training set includes high-energy EOS data. The NN trained only on energies displays a sign of overfitting after about 50,000 steps, while the one trained on energy-force data shows comparable training and testing errors (with or without EOS data) until the end of the 420,000 optimization run.

weight values have little effect on the resulting NN accuracy and that NN snapshots saved during an optimization run provide similar description of EOS, defect energy, and phonons (Figure S4 in Ref. [34]). Overfitting is avoided by keeping the data to parameter ratio above 10:1 and using L_2 regularization with $10^{-8} - 10^{-6}$ values. Figure 4 shows typical rates of convergence in energy and energy-force training runs.

7.4 Stratified training

The construction of NNs for multielement systems in MAISE follows a stratified scheme introduced and examined in our previous study [34]. It differs from the traditional approach in that we fit NN weights in a hierarchical fashion from the bottom up, first for elements, then for binaries, and so on. The intact description of the subsystems, as the NN is expanded to more elements, is achieved via the use of a constrained NN architecture. The concept of stratification has been used in the development of classical and tight-binding models [129, 130, 131] but has not received much attention yet in the development of machine learning potentials.

Under ideal conditions - given a complete basis for representing atomic environments within a large cutoff sphere, unlimited number of adjustable parameters and reference data, and a powerful fitting algorithm - a multielement NN with fully optimized elemental and interspecies weights is expected to accurately map the PES for all subsystems. In practice, the use of approximations leads to the following problem. Suppose one wishes to fit a model describing A, B, and AB phases given three datasets of A, B, and AB structures. Let's say that the PES of element A happens to be trivial and can be approximated with negligible error in the region spanned by the A data. If one now fits all parameters simultaneously to the full A, B, and AB dataset the larger error will be distributed across all elemental and binary systems. In other words, the addition of B and AB data unphysically alters the description of the elemental A phases. It should be noted that the constrained NN architecture does account for the change in the interaction strength between

A atoms induced by the presence of B atoms because the AA/AAA inputs are mixed in with the AB/AAB/ABB inputs via neurons' non-linear activation functions.

In a study of a particular composition, e.g., MgO, it would not make much sense to start the parameterization with the elements because they will not be encountered in charge-neutral forms or relevant coordinations in MgO structures. With our primary interest in the exploration of full compositions in multiple binary/ternary metal alloys, we have relied on the stratified scheme to build sets of reusable NN models. Our extensive tests have shown that the constraints in the adopted NN architectures do not introduce any appreciable errors for the considered chemical systems [34].

In addition to having a more sound foundation, the stratification procedure significantly accelerates the creation of NN libraries. For example, the full training of a binary AB model on all A, B, and AB data takes about the same time as the sequential training of A, B, and AB models on the corresponding data subsets. However, for an extended block of A, B, and C elements, the standard approach involves the fitting of AC and BC NNs from scratch, while the inheritance of A and B weights in the stratified scheme reduces the total fitting time by at least a factor of two. The speed-up increases dramatically as more elements are added and ternary models are built.

Users can choose the full or stratified scheme with the JOBT flag in the 'setup' file. In the latter case, substituent models should be placed in the working directory, e.g., 'Cu.dat' and 'Pd.dat' for fitting the Cu-Pd binary NN, or 'CuPd.dat', 'CuAg.dat', and 'PdAg.dat' for fitting the Cu-Pd-Ag ternary NN. Presently, MAISE allows for training NN models with up to three elements. While the treatment of systems with more elements is possible conceptually, the practical cost of data generation and parameter optimization becomes expensive.

7.5 Generalized stratified training

In order to extend the stratified procedure to materials with more complex interactions and an arbitrary number of elements, we have considered more flexible NN architectures that still preserve the intact description of the subsystems. Compared to the original stratified NN layout [34], it involves addition of new neurons, shown as green units in Figure 5, with different connection patterns and conditions.

The schematic of a 'stratified+' binary NN (top row in Figure 5) illustrates that as long as there are no connections *from* the inputs or neurons in the elemental subnets *to* the inserted neurons, the new adjustable weights do not alter the signal processing for pure elemental structures. Despite the added flexibility, the NN still does not allow the proper fitting of interactions in compounds with more than three chemical elements. Indeed, the adjustable parts of such NNs involve 60% of inputs in binaries (top right box in Figure 5), 11% of inputs in ternaries (caption of Figure 5) and none for systems with more elements. In our previous discussion [34], we incorrectly attributed this limitation to the use of pair and triplet symmetry functions. This restriction is actually imposed not by the particular geometric representation of the atomic environments [21, 132, 133] but rather by the NN architecture, and can be lifted as follows.

The 'stratified±' expansion (bottom row in Figure 5) introduces semi-adjustable links even in the inherited parts of the merged NN. We add neurons in pairs, coupling the two weights incoming from each subsystem input to have opposite values while coupling the two outgoing weights to be the same. For a purely elemental structure, the interspecies input values are zero and the net signal (at neuron 5) from each elemental input (1) passed through the paired neurons (3&4) will be zero as well regardless of the coupled weight *magnitudes*. For a binary structure, the non-zero binary inputs multiplied by fully unconstrained weights will unbalance the elemental signals because of the non-linear nature of the activation function resulting in a non-zero contribution at neuron 5

that depends on *both* elemental and binary (semi)adjustable weights.

The set of new partially constrained weights shown in yellow in Figure 5 enables the stratified \pm NN to better capture the screening and charge transfer effects as well as describe interactions in systems with an unlimited number of species. In a trial implementation, we imposed the constraint by penalizing the mismatch between the coupled weights as $\sum_N \sigma(w_{1,N} \pm w_{2,N})^2$. We have observed no need to adjust the σ penalty factor during the NN optimization, as the differences between coupled weight magnitudes become negligible after a few dozen training steps; near the end of optimization, we set the magnitudes to their average and keep them fixed without any appreciable effect on the error. To the best of our knowledge, this semi-constrained solution for systematically expanding NN features has not been considered in the field of materials modeling. It adds to the collection of alternative NN architectures proposed in recent years for more general applications, such as progressive [134], dynamically expandable [135], and implanted [136] NNs.

One way to determine whether the use of the expanded NN architectures is warranted is to reoptimize the standard stratified NN without any constraints on the full dataset. A significant reduction in the training and testing errors would indicate the need for additional NN flexibility. In our studies of metal alloys, the error reductions are usually in the 0-15% range (e.g., see Figure 4 in Ref. [34]). Our preliminary tests have shown that both stratified+ and \pm architectures end up with errors about midway between those in the stratified and full NNs. In order to quantify the improvements arising from the additional degrees of freedom in each scheme, we plan to investigate more challenging systems comprised of different element types in future studies.

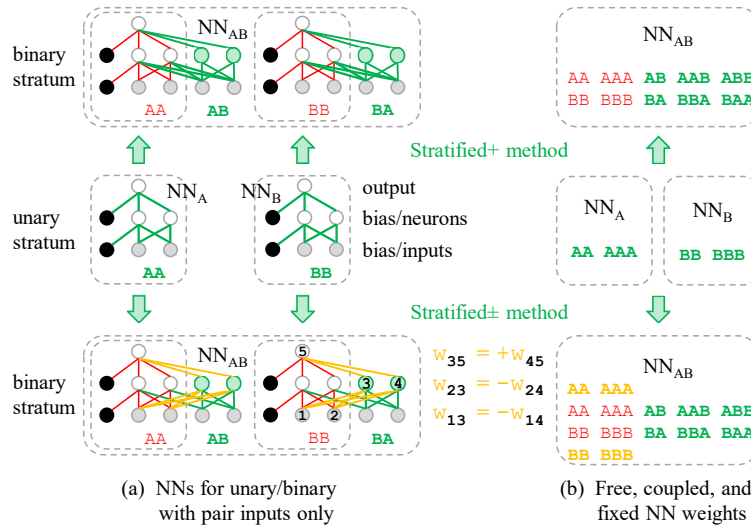


Figure 5: Schematic illustration of stratified+ (top row) and stratified \pm (bottom row) NN architectures for a binary chemical system. The expansion of the original stratified architecture is done with the addition of new neurons shown in green. The weights of elemental NNs (middle row) are copied and kept fixed in all stratified variations. Free, coupled, and fixed weights are shown in green, yellow, and red, respectively. (a) Connections in a simplified NN with one hidden layer and only pair inputs. The partial constraints shown in yellow and explained in the main text ensure intact description of the elemental structures. (b) Color-coded degrees of weight constraints in NNs with pair and triplet inputs. The original and stratified+ schemes have 60% adjustable weights in the first layer in binaries, 11% in ternaries (e.g., only the last one among AA, AB, AC, AAA, AAB, AAC, ABB, ACC, ABC, see Ref. [34]), and none in quaternaries. The stratified \pm architecture can be used for an arbitrary number of chemical elements.

8 MAISE-NET: automated generator of neural networks

Generation of reference structures suitable for tuning machine learning models has been explored in numerous studies [26, 27, 37, 43, 124, 137, 138, 139, 140, 141, 142, 123, 125, 126, 143, 127, 144]. *Ab initio* MD has been a particularly popular approach to sample physically meaningful configurations [26, 27]. In our previous work, we argued that datasets created with MD might not have the sufficient representation of diverse environments probed in global structure searches [34]. Our evolutionary sampling protocol proposed in 2017 served as a basis for an unsupervised creation of diverse datasets, and our NN models trained on such data have been successfully used in structure prediction [40, 19, 20]. A similar approach was developed by Dolgirev *et al.* [145]. Several strategies to improve the mapping of configuration spaces have been developed in recent years, e.g., normal mode sampling [142], active learning-based models [125, 126], enhanced sampling [127], *ab initio* random structure searching [123, 124], and entropy-maximization approach [143]. A number of studies have shown the benefit of iterating the generation of data and the parameterization of models [26, 34, 41, 123, 124, 125, 126, 144].

The generalized sampling protocol implemented in the MAISE-NET wrapper [99] relies on the evolutionary search, structure analysis, and NN fitting features in MAISE to construct training datasets in an automated iterative fashion. It has been developed over several studies to deal with systems of increasing complexity. In our early investigation of crystal structure phases of relatively simple Cu-Pd-Ag metals, it was sufficient to generate each of the unary, binary, and ternary datasets in a single cycle, as the NNs trained on this data showed robust performance [34]. An accurate description of Cu-Pd-Ag and Au NPs required an iteration to sample cluster geometries with pretrained NNs [19, 20]. Our ongoing studies have been dedicated to predicting high-pressure alloy phases and involve several cycles to include unusual motifs stabilized under compression.

An overview of the MAISE-NET operation is presented in Figure 6. A database construction run starts with building a precursive dataset followed by cycles of data generation and NN model training. The complete data generation process is carried out in multiple steps as follows:

(a) *Basic data generation (optional)*: If instructed by the user, the script generates a single atom reference and sets of EOS data for small clusters with 2-4 atoms and select high-symmetry prototypes preoptimized for the considered element(s). While being optional, these reference sets, called collectively as EOS0, are essential for teaching the NN to disfavor configurations with unphysically short or long interatomic distances.

(b) *Preliminary DFT-level evolutionary sampling*: MAISE-NET sets up short evolutionary MAISE runs initialized with random structures. As described in Ref. [34], the local DFT optimization of each population member for a few ionic steps is followed by an accurate static evaluation of the energy and forces of the resulting configuration. The small set of structures in this cycle 0 samples the walls of multiple basins and is sufficient for a rough approximation of the PES.

(c) *NN model training*: The collection of all available high-accuracy DFT data is parsed and a NN model is built. Various system- and cycle-dependent fitting specifications can be defined in the setup file, e.g., the energy or energy-force training type, the number of steps for each training type, etc.

(d) *NN-driven generation of DFT data*: MAISE-NET launches MAISE evolutionary runs to randomly generate and locally optimize new structures using the latest NN model. Compared to step (b), it proved to be unnecessary to proceed beyond the first ES generation because small unit cells with 1-8 atoms have a chance to converge to the global minimum with full local optimization affordable at the NN level. After the uniqueness of the obtained minima is verified through the structure comparison feature in MAISE and they are accepted in the pool based on a weighting

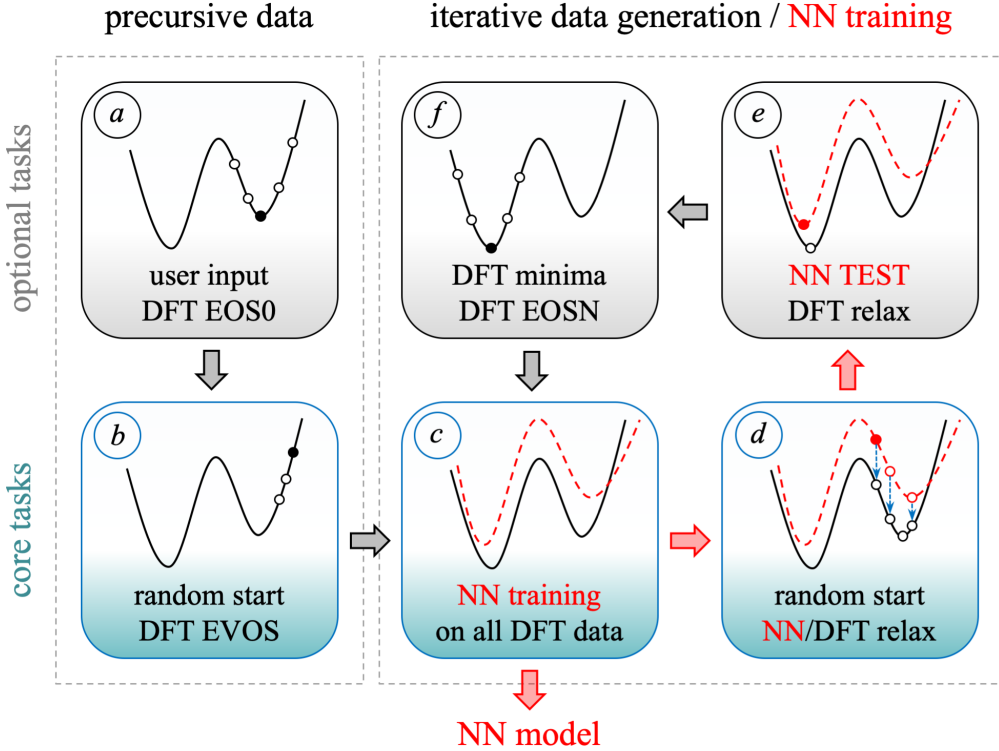


Figure 6: A flowchart of the MAISE-NET automated generation of reference data and construction of NN models. The core and optional tasks are shown in blue and grey boxes, respectively. Black and red curves represent the reference DFT PES and its NN approximation, respectively. Data produced in steps (a,b) is used to launch an iterative process shown in steps (c-f). A detailed description of all stages is given in the text.

factor favoring low-enthalpy structures, the corresponding relaxation paths are examined to extract several intermediate structures per minimum. The target total number of generated structures per cycle, referred to as 'EVOS' data, is specified in the setup file.

(e) *NN model test and TEST data (optional)*: If instructed by the user, MAISE-NET launches a proper evolutionary ground state search using the NN model trained in step (c). The resulting NN-based minima are then optimized at the DFT level. A detailed report is compiled on the symmetry and enthalpy of the resulting minima at the NN and DFT levels. The user has an option to include the DFT energies and forces of the NN- and DFT-based minima into the dataset for the NN training in subsequent cycles. The data will be added to the collection of training data as 'TEST' data. Although generation of the TEST data during the model construction run is optional, the script has the feature to perform this evolutionary search test for an existing NN model as an independent functionality.

(f) *DFT EOSN data generation (optional)*: If instructed by the user, a small set of EOS data is generated for unique DFT-optimized minima obtained in each cycle and added to the pool of training data for the next cycles as 'EOSN' data.

Steps (c) through (f) are repeated for a user-specified number of cycles, with a NN model trained from scratch on all collected DFT data at the end of each iteration. The run can be terminated or extended by the user at each iteration depending on whether a satisfactory accuracy for the NN model is achieved. While steps (a), (e), and (f) are optional, our tests for elemental, binary, and ternary metal systems have indicated that addition of these datasets significantly improves the NN

model suitability for ground state searches in terms of accuracy and reliability. Generation of a typical training dataset of $\sim 5,000$ structures with the MAISE-NET script required roughly 20, 30, and 40 thousand CPU hours of DFT calculations for elemental, binary, and ternary metallic compounds, respectively. The higher DFT calculation cost for each binary and ternary systems is primarily due to the increased number of DFT calculations for structures with larger unit cells. Figure 7 illustrates the distribution of data and NN accuracy for Cu-Ag.

The end-to-end NN construction depends on a large number of parameters and can be a daunting task for new users. With this in mind, we have developed MAISE-NET to have the following features.

Easy customization MAISE-NET can be run with both Python 2 and 3 version families out-of-the-box without requiring any external modules to be installed. It includes well-tested 'setup' templates for developing elemental, binary, and ternary NN models. All key functionalities can be tuned by adjusting 'setup' parameters listed in Table A9. Upon detection of user-provided NN models for the relevant subsystems, the script performs the NN fitting in the stratified fashion.

Complete automation Once the run is configured, the data generation and NN construction can proceed without any further user input or supervision. In particular, the script makes sure that DFT data is collected only from successfully finished VASP calculations.

Full transparency An extensive set of messages is produced and sent into standard output/screen to notify the user about the progress of the run. The most important messages are saved in the 'output.dat' file. A comprehensive summary is generated to give the user a detailed account about the generated dataset.

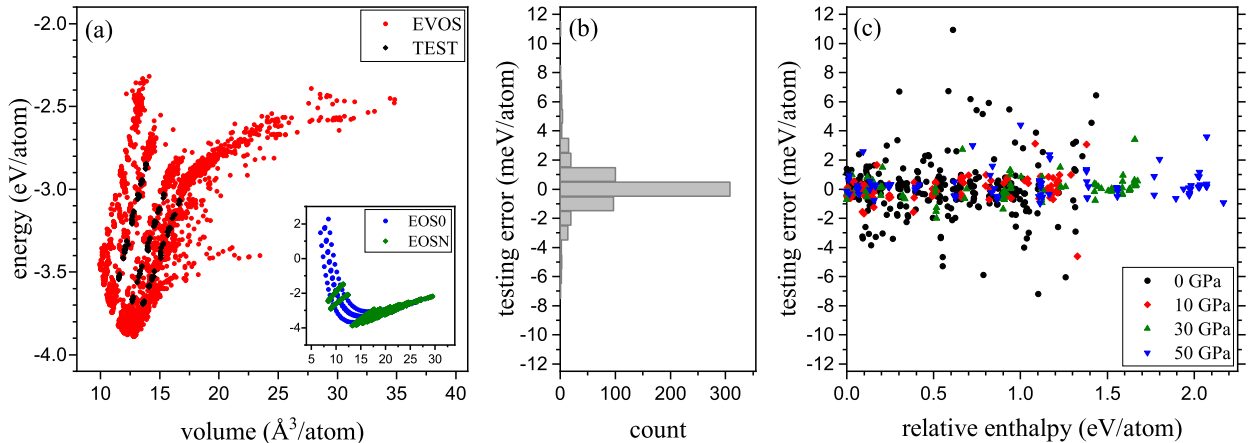


Figure 7: Characteristics of the generated dataset and accuracy of the constructed NN model for the Cu-Ag binary. (a) Distribution of the generated dataset for various data types: EVOS (evolutionary data), TEST (NN model testing results), EOS0 (basic data generated before zeroth cycle), and EOSN (EOS data generated during the evolutionary run). (b) Histogram of energy errors the testing set. (c) Distribution of testing errors as a function of the enthalpy difference relative to the lowest-enthalpy phase at each pressure.

9 Library of neural network models

A library of select NN and empirical potentials is provided with the distribution in the 'models/' directory. Model file names specify the interaction type (a NN or a traditional potential), dimensionality of the data used to parameterize the model (0 for crystals and clusters or 3 for crystals only), and the generation/version number. Model file headers list information about models' authorship, architecture, performance, etc. The body of the NN files contain bias and weight values. Finally, the end of the files specifies the symmetry function basis chosen for the model.

We have recently started building a new generation of NN models (gen2) for a large set of metals to allow the prediction of stable alloys under ambient and high pressures. The use of MAISE-NET with standardized settings ensures that we can create a library of models in the stratified fashion. Figure 8 shows the accuracy of the new generation of NNs tested to perform well in structure searches up to 30 GPa pressure.

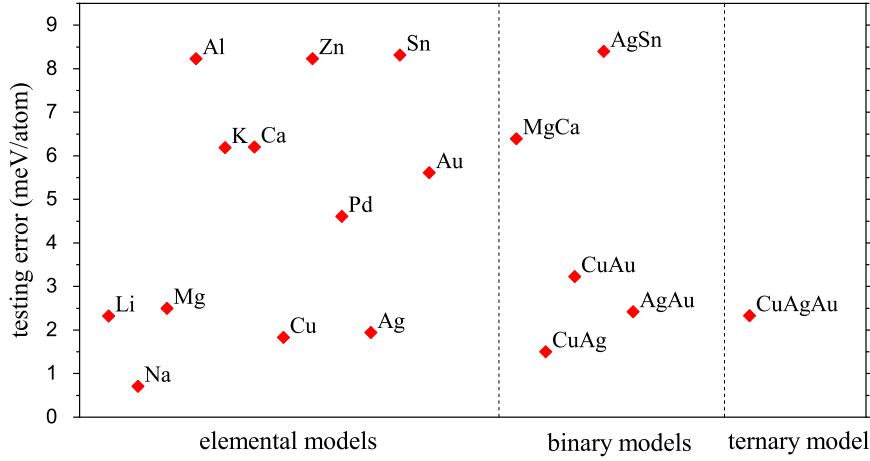


Figure 8: Testing error for available second-generation NN interatomic potentials constructed with the MAISE-NET script.

10 Performance and efficiency

Benchmarking results reported in our previous studies [34, 40, 19, 20] have demonstrated the levels of speed and accuracy generally expected from the constructed NN models. For systems with 50–100 atoms, calculations performed with the order- N NNs were found to be 10^4 – 10^5 times faster than with the order- N^3 DFT and about 10^2 times slower than the order- N empirical potentials [146, 35, 147, 148]. The two most demanding computational tasks, the NN training and the NN use in structure simulations, are parallelized with OpenMP over the total number of structures in the reference dataset in the former case and over the number of atoms in the latter one. Figure 9 illustrates that the parallelization efficiency is system-dependent and can be up 90% on 16 cores and 70% on 32 cores.

As overviewed in Section 9, the overall accuracy for most developed models ranges between 2 and 10 meV/atom in the considered systems with up to three metals. The DFT formation defect energies are typically reproduced within 0.1–0.2 eV/defect (see Figure 10), which is consistent with the NN errors per atom (see discussion in Ref. [34]). The accurate description of forces with the NNs allows one to identify dynamically unstable structures and obtain accurate evaluations

of relative phase stability at elevated temperatures by including vibrational entropy corrections (Figure 5 in Ref. [20] and Figure 10 in the present work). It has been encouraging to observe practically the same accuracy of NNs trained in the full and stratified fashions.

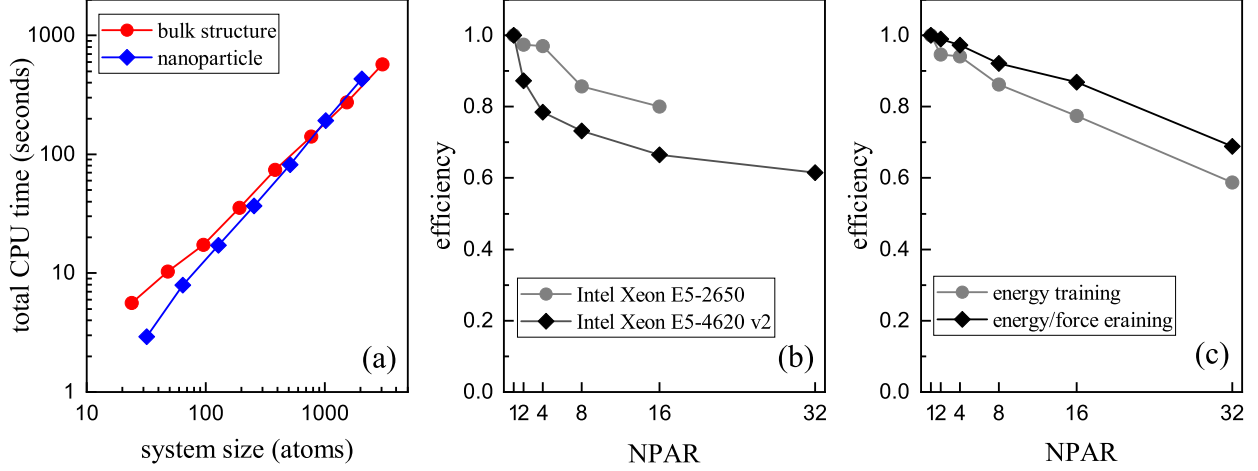


Figure 9: MAISE performance in structure relaxation and NN model training. (a) Total CPU time for the relaxation of bulk (red circles) and NP (blue diamonds) Au structures performed on a 32-core Intel Xeon Gold 5218 @ 2.30 GHz compute node. (b) Parallelization efficiency of MAISE for local optimization of a 1024-atom Au crystal structure computed on a 16-core Intel Xeon E5-2650 @ 2.00 GHz (grey circles) and a 32-core Intel Xeon E5-4620 v2 @ 2.60 GHz (black diamonds). The dynamic allocation in OpenMP helps distribute the load for processing atoms with different numbers of neighbors. (c) Parallelization efficiency of training a NN model on energy-only (grey circles) and energy-force (black diamonds) data, performed on a 32-core Intel Xeon Gold 5218 @ 2.30 GHz compute node.

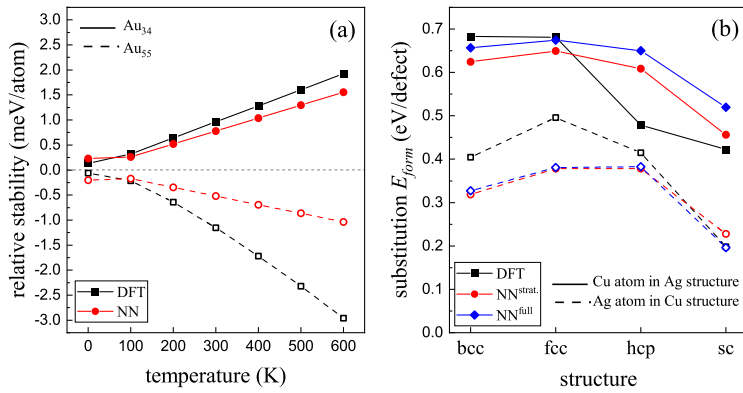


Figure 10: Accuracy of the NN models constructed with MAISE in the evaluation of different properties. (a) Vibrational entropy corrections to the relative stability between two low-energy NPs for two sizes, Au₃₄ and Au₅₅[20]. (b) Substitutional defect formation energies for Cu-Ag binary structures evaluated with stratified (red circles) and full (blue diamonds) NN models and compared to the DFT values (black squares).

The most important quality measure of NNs developed in our studies has been their performance in structure prediction [40, 19, 20]. We carried out a systematic comparison of NN models and traditional potentials against the DFT, which appears to be the largest of the kind so far, to quantify their ability to resolve low-energy configurations in global structure searches [20]. By examining up to 60 lowest-energy candidates for each size in the $\text{Au}_{30}\text{-}\text{Au}_{80}$ NP range, we established that NNs (6.5 meV/atom accuracy) are far better suited to guide *ab initio* ground state search than the Gupta, Sutton-Chen, or embedded atom model (estimated 30 meV/atom accuracy). The large number of NP configurations with close energies makes it difficult to conclusively determine the DFT minimum with either approach but the use of the NNs instead of the traditional potentials reduces the number of structures needed to be re-evaluated at the DFT level by at least 1-2 orders of magnitude. Moreover, the good correspondence between the NN and DFT atomic forces allowed us to introduce a hybrid NN+DFT approach that significantly improves the search reliability. Application of NN models with 2-10 meV/atom accuracy to bulk crystals is expected to be far more effective for identifying the DFT ground states because of the simpler PES near the global minimum in systems without surfaces.

11 Summary

In this work, we have reviewed notable predictions and present capabilities of MAISE. The list of eight crystal structure predictions made at the DFT level and confirmed in concurrent or following experiments is presented in Section 2. The identification of possible synthesizable Mg-Ca phases with global structure searches at the NN level[34], which appears to be the first example of new thermodynamically stable crystalline compounds predicted in this fashion, is discussed in Section 2. Key aspects of the evolutionary optimization implemented in MAISE for crystals, films, and clusters are described in Section 6.

The main feature of the package is the construction of NN interaction models for use in structure prediction (Section 7). We outline our protocols for configuration space sampling and NN training that ensure the robustness of the DFT PES mapping. In particular, we introduce expanded stratified schemes that allow the construction of NN models in a hierarchical fashion for an arbitrary number of chemical elements. All stages of the iterative NN development are handled with an automated MAISE-NET wrapper (Section 8). The script has been used in our ongoing effort to build a new generation of NN models (Section 9). So far, NNs for 12 metals, 5 binary alloys, and 1 ternary alloy with an accuracy in the 2-9 meV/atom range have been tested in unconstrained structure searches at pressures up to 30 GPa. Section 5 illustrates MAISE and NN performance in local structure relaxations, MD simulations, and phonon calculations. MAISE, MAISE-NET, and developed NN models are available for download on Github [98, 99].

12 Acknowledgment

We acknowledge the NSF support (Award No. DMR-1821815) and the Extreme Science and Engineering Discovery Environment computational resources [149] (NSF award No. ACI-1548562, project No. TG-PHY190024). We thank Igor Mazin, Gábor Csányi, and Michele Ceriotti for insightful discussions.

Appendix A Setup parameters for various MAISE features

This section lists key setup parameters for evolutionary global structure optimization, local structure optimization, MD simulations, data parsing, and NN training with MAISE as well as key setup parameters for the automated NN model construction with MAISE-NET. The following tables include a minimal set of parameters, i.e., those which need to have a defined value for the code to operate properly.

flag	description
JOBT	job type: structure relaxation (20)
NPAR	number of cores for parallel run
NDIM	dimensionality of unit cell: crystal (3); cluster (0)
MITR	maximum number of cell optimization steps
RLXT	cell optimization type: force only (2); full cell (3); volume (7)
PGPA	external pressure in GPa
ETOL	error tolerance for cell optimization convergence
COUT	output options E: final (00); first/final (01); all steps (02); EF: final (10); first/final (11); all steps (12)
MINT	minimizer type: BFGS2 (0); CG-FR (1); CG-PR (2); steepest descent (3)

Table A3: Setup parameters for local structure optimization.

flag	description
JOBT	job type: molecular dynamics (21)
MDTP	MD run type: <i>NVE</i> (10); <i>NVT</i> (20); <i>NPT</i> (30); isobaric-isothermal (40)
NPAR	number of cores for parallel run
TMIN	starting temperature of the simulation
TMAX	final temperature of the simulation
TSTP	temperature increment during the simulation
DELT	integration time step in fs
NSTP	number of integration steps per temperature
CPLTP	thermostat coupling constant
CPLP	barostat coupling constant
ICMP	isothermal compressibility in 1/GPa

Table A4: Setup parameters for MD simulations.

flag	description
JOBT	job type: phonon calculations (22)
DISP	size of the displacement made to each atom in angstroms
NPAR	number of cores for parallel run
NDIM	dimensionality of the unit cell: crystal (3); cluster (0)

Table A5: Setup parameters for phonon calculations.

flag	description
JOBT	evolutionary search: run (10); soft exit (11); hard exit (12); analysis (13)
NMAX	maximum number of atoms
MMAX	maximum number of neighbors within cutoff radius
NSPC	number of species types
TSPC	species types
ASPC	atom number of each species in evolutionary searches
CODE	MAISE-INT (0); VASP-EXT (1); MAISE-EXT (2)
QUET	queue type: torque (0); slurm (1)
NDIM	structure type: crystal (3); film (2); cluster (0)
LBOX	box size for cluster calculations (ignored for crystals)
NPOP	population size
SITR	starting iteration
NITR	number of iterations
TINI	starting options if SITR=0
TIME	max time per relaxation
PGPA	pressure in GPa
DENE	energy/atom window for selecting distinct structures
SCUT	RDF difference for selecting distinct structures
TETR	random using TETRIS
PLNT	seeded
PACK	biased
BLOB	random using blob shape
MATE	crossover using two halves
SWAP	crossover using core-shell
RUBE	Rubik's cube operation
REFL	symmetrization via reflection
INVS	symmetrization via inversion
CHOP	chop to make facets
MUTE	distortion
ELPS	cluster ellipticity
MCRS	crossover: mutation rate
SCRS	crossover: swapping rate
LCRS	crossover: mutation strength for lattice vectors
ACRS	crossover: mutation strength for atomic positions
SDST	distortion: swapping rate
LDST	distortion: mutation strength for lattice vectors
ADST	distortion: mutation strength for atomic positions
SEED	starting seed for the random number generator (0 for system time)

Table A6: Setup parameters for evolutionary search.

flag	description
JOBT	job type: data parsing (30)
NPAR	number of cores for parallel training or cell simulation
TEFS	parsing for: E (0); EF (1)
FMRK	fraction of atoms that will be parsed to use for EF training
NSPC	number of element types for dataset parsing and training
TSPC	atomic number of the elements specified with NSPC tag
NSYM	number of the BP symmetry functions for parsing data
NCMP	the length of the input vector of the neural network
ECUT	parse only this fraction of lowest-energy structures (from 0 to 1)
EMAX	maximum energy from the lowest-energy structure that is parsed
FMAX	will not parse data with forces larger than this value
RAND	random seed for the parsing: time (0); seed value (+); no randomization (-)
DEPO	path to the DFT datasets to be parsed
DATA	location of the parsed data to write the parsed data

Table A7: Setup parameters for data parsing.

flag	description
JOBT	training type: full training (40); stratified training (41)
NPAR	number of cores for parallel training
MINT	the optimizer algorithm for neural network training
MITR	number of the optimization steps for training
ETOL	error tolerance for training
TEFS	training target value: E (0); EF (1)
NSPC	number of element types for dataset parsing and training
TSPC	atomic number of the elements specified with NSPC tag
NSYM	number of the BP symmetry functions for parsing data
NCMP	the length of the input vector of the neural network
NTRN	number of structures used for training (negative number means percentage)
NTST	number of structures used for testing (negative number means percentage)
NNNN	number of hidden layers (does not include input vector and output neuron)
NNNU	number of neurons in hidden layers
NNGT	activation function type for the hidden layers' neurons: linear (0); tanh (1)
LREG	regularization parameter
SEED	rand seed for generating NN weights (0 for system time)
DATA	location of the parsed data to read from for training
OTPT	directory for storing model parameters in the training process
EVAL	directory for model testing data

Table A8: Setup parameters for training of NN models.

flag	description
JOBT	job type: basic data generation (80); evolutionary data generation (81); test run (87); pause (88); exit (89)
TSPC	atomic number of the elements
QUET	queue type: torque (0); slurm (1); IBM-lsf (2)
LBOX	unit cell size: should be non-zero for BASIC data
MAXJ	maximum number of DFT jobs to be submitted at once
ECUT	energy cut-off for DFT (0 = VASP default)
PREC	precision of the DFT run (e.g., norm,acc)
KDNS	K-mesh density for DFT runs
SMER	VASP ISMEAR
SIGM	VASP SIGMA (for REFS and CLST data will be set to 0.01)
LREG	regularization parameter
NNNU	number of neurons in hidden layers
NNGT	activation function type for the hidden layers' neurons: linear (0); tanh (1)
NPAR	number of cores for parallel parsing
NSYM	number of the BP symmetry functions for parsing data
RCUT	BP symmetry function cut-off radius: 6 Å (0); 7.5 Å (1)
FMRK	ratio of atomic forces for training
SITR	starting cycle (0 for full run)
NITR	final cycle
DATA	desired number of structures per cycle (1+)
aspC	list of number of atoms/unit cell (for cycle 0)
npop	list of population size for evolution runs (for cycle 0)
mitr	number of training steps (for cycle 0)
tefs	type of training at each round
ASPC	list of number of atoms/unit cell (for cycles 1+)
NPOP	population size for evolution runs (for cycles 1+)
ITER	relaxation steps for NN-based search
MITR	number of training steps (for cycles 1+)
TEFS	type of training at each round (for cycles 1+)
EXTR	extended force training factor when cycle = NITR

Table A9: Setup parameters for automated model construction with MAISE-NET.

References

- [1] A N Kolmogorov, S Shah, E R Margine, A F Bialon, T Hammerschmidt, and R Drautz. New superconducting and semiconducting Fe-B compounds predicted with an *Ab initio* evolutionary search. *Physical Review Letters*, 105(21):217003, 2010.
- [2] D. M. Deaven and K. M. Ho. Molecular geometry optimization with a genetic algorithm. *Physical Review Letters*, 75(2):288–291, 1995.
- [3] Scott M. Woodley, Peter D. Battle, Julian D. Gale, and C. Richard A. Catlow. The prediction of inorganic crystal structures using a genetic algorithm and energy minimisation. *Physical Chemistry Chemical Physics*, 1(10):2535–2542, 1999.
- [4] Colin W. Glass, Artem R. Oganov, and Nikolaus Hansen. Uspexevolutionary crystal structure prediction. *Computer Physics Communications*, 175(11):713 – 720, 2006.
- [5] Artem R Oganov and Colin W Glass. Evolutionary crystal structure prediction as a tool in materials design. *Journal of Physics Condensed Matter*, 20(6):64210, 2008.
- [6] S. M. Woodley and C. R.A. Catlow. Structure prediction of titania phases: Implementation of Darwinian versus Lamarckian concepts in an Evolutionary Algorithm. *Computational Materials Science*, 45(1):84–95, 2009.
- [7] S M Woodley, Alexey A Sokol, and C Richard A Catlow. Structure Prediction of Inorganic Nanoparticles with Predefined Architecture using a Genetic Algorithm. *Zeitschrift für anorganische und allgemeine Chemie*, 630(1314):2343–2353, 2004.
- [8] Sandro E Schönborn, Stefan Goedecker, Shantanu Roy, and Artem R Oganov. The performance of minima hopping and evolutionary algorithms for cluster structure prediction. *Journal of Chemical Physics*, 130(14):144108, 2009.
- [9] Yanchao Wang, Jian Lv, Li Zhu, and Yanming Ma. CALYPSO: A method for crystal structure prediction. *Computer Physics Communications*, 183(10):2063–2070, 2012.
- [10] Silvia Bahmann and Jens Kortus. Evoevolutionary algorithm for crystal structure prediction. *Computer Physics Communications*, 184(6):1618 – 1625, 2013.
- [11] William W Tipton and Richard G Hennig. A grand canonical genetic algorithm for the prediction of multi-component phase diagrams and testing of empirical potentials. *Journal of Physics: Condensed Matter*, 25(49):495401, nov 2013.
- [12] Giancarlo Trimarchi, Arthur J Freeman, and Alex Zunger. Predicting stable stoichiometries of compounds via evolutionary global space-group optimization. *Physical Review B - Condensed Matter and Materials Physics*, 80(9):92101, 2009.
- [13] Qiang Zhu, Vinit Sharma, Artem R. Oganov, and Ramamurthy Ramprasad. Predicting polymeric crystal structures by evolutionary algorithms. *Journal of Chemical Physics*, 141(15):154102, 2014.
- [14] Zhong-Li Liu. Muse: Multi-algorithm collaborative crystal structure prediction. *Computer Physics Communications*, 185(7):1893 – 1900, 2014.

[15] S V Lepeshkin, V S Baturin, Yu. A Uspenskii, and Artem R Oganov. Method for Simultaneous Prediction of Atomic Structure and Stability of Nanoclusters in a Wide Area of Compositions. *Journal of Physical Chemistry Letters*, 10(1):102–106, 2019.

[16] Patrick Avery, Cormac Toher, Stefano Curtarolo, and Eva Zurek. Xtalopt version r12: An open-source evolutionary algorithm for crystal structure prediction. *Computer Physics Communications*, 237:274 – 275, 2019.

[17] A. N. Kolmogorov, S. Shah, E. R. Margine, A. K. Kleppe, and A. P. Jephcoat. Pressure-driven evolution of the covalent network in CaB₆. *Physical Review Letters*, 109(7):75501, 2012.

[18] Sheena Shah and Aleksey N Kolmogorov. Stability and superconductivity of Ca-B phases at ambient and high pressure. *Physical Review B - Condensed Matter and Materials Physics*, 88(1), 2013.

[19] Samad Hajinazar, Ernesto D. Sandoval, Aiden J. Cullo, and Aleksey N. Kolmogorov. Multitribe evolutionary search for stable CuPdAg nanoparticles using neural network models. *Physical Chemistry Chemical Physics*, 21(17):8729–8742, 2019.

[20] Aidan Thorn, Javier Rojas-Nunez, Samad Hajinazar, Samuel E. Baltazar, and Aleksey N. Kolmogorov. Toward ab initio ground states of gold clusters via neural network modeling. *The Journal of Physical Chemistry C*, 123(50):30088–30098, 2019.

[21] Jörg Behler and Michele Parrinello. Generalized Neural-Network Representation of High-Dimensional Potential-Energy Surfaces. *Physical Review Letters*, 98(14):146401, 2007.

[22] Jörg Behler, Roman Martoák, Davide Donadio, and Michele Parrinello. Metadynamics simulations of the high-pressure phases of silicon employing a high-dimensional neural network potential. *Physical Review Letters*, 100(18):185501, 2008.

[23] Hagai Eshet, Rustam Z. Khaliullin, Thomas D. Kühne, Jörg Behler, and Michele Parrinello. *Ab initio* quality neural-network potential for sodium. *Physical Review B - Condensed Matter and Materials Physics*, 81(18):184107, 2010.

[24] Jörg Behler. Neural network potential-energy surfaces in chemistry: A tool for large-scale simulations. *Physical Chemistry Chemical Physics*, 13(40):17930–17955, 2011.

[25] Nongnuch Artrith, Tobias Morawietz, and Jörg Behler. High-dimensional neural-network potentials for multicomponent systems: Applications to zinc oxide. *Physical Review B - Condensed Matter and Materials Physics*, 83(15):153101, 2011.

[26] Nongnuch Artrith and Jörg Behler. High-dimensional neural network potentials for metal surfaces: A prototype study for copper. *Physical Review B - Condensed Matter and Materials Physics*, 85(4):45439, 2012.

[27] Nongnuch Artrith, Björn Hiller, and Jörg Behler. Neural network potentials for metals and oxides - First applications to copper clusters at zinc oxide. *Physica Status Solidi (B) Basic Research*, 250(6):1191–1203, 2013.

[28] Tobias Morawietz and Jörg Behler. A full-dimensional neural network potential-energy surface for water clusters up to the hexamer. *Zeitschrift fur Physikalische Chemie*, 227(11):1559–1581, 2013.

- [29] J. Behler. Representing potential energy surfaces by high-dimensional neural network potentials. *Journal of Physics Condensed Matter*, 26(18):183001, 2014.
- [30] Suresh Kondati Natarajan, Tobias Morawietz, and Jörg Behler. Representing the potential-energy surface of protonated water clusters by high-dimensional neural network potentials. *Physical Chemistry Chemical Physics*, 17(13):8356–8371, 2015.
- [31] Jörg Behler. Perspective: Machine learning potentials for atomistic simulations. *Journal of Chemical Physics*, 145(17):170901, 2016.
- [32] Nongnuch Artrith and Alexander Urban. An implementation of artificial neural-network potentials for atomistic materials simulations: Performance for tio2. *Computational Materials Science*, 114:135 – 150, 2016.
- [33] Alireza Khorshidi and Andrew A. Peterson. Amp: A modular approach to machine learning in atomistic simulations. *Computer Physics Communications*, 207:310–324, 2016.
- [34] Samad Hajinazar, Junping Shao, and Aleksey N. Kolmogorov. Stratified construction of neural network based interatomic models for multicomponent materials. *Physical Review B*, 95(1):14114, 2017.
- [35] Khosrow Shakouri, Jörg Behler, Jörg Meyer, and Geert Jan Kroes. Accurate Neural Network Description of Surface Phonons in Reactive Gas-Surface Dynamics: $\text{N}_2 + \text{Ru}(0001)$. *Journal of Physical Chemistry Letters*, 8(10):2131–2136, 2017.
- [36] Jörg Behler. First Principles Neural Network Potentials for Reactive Simulations of Large Molecular and Condensed Systems. *Angewandte Chemie - International Edition*, 56(42):12828–12840, 2017.
- [37] Volker L. Deringer and Gábor Csányi. Machine learning based interatomic potential for amorphous carbon. *Phys. Rev. B*, 95:094203, Mar 2017.
- [38] Brian Kolb, Levi C. Lentz, and Alexie M. Kolpak. Discovering charge density functionals and structure-property relationships with prophet: A general framework for coupling machine learning and first-principles methods. *Scientific Reports*, 7(1):1192, Apr 2017.
- [39] Kristof Schütt, Pieter-Jan Kindermans, Huziel Enoc Sauceda Felix, Stefan Chmiela, Alexandre Tkatchenko, and Klaus-Robert Müller. Schnet: A continuous-filter convolutional neural network for modeling quantum interactions. In I. Guyon, U. V. Luxburg, S. Bengio, H. Wallach, R. Fergus, S. Vishwanathan, and R. Garnett, editors, *Advances in Neural Information Processing Systems 30*, pages 991–1001. Curran Associates, Inc., 2017.
- [40] Wilfredo Ibarra-Hernández, Samad Hajinazar, Guillermo Avendaño-Franco, Alejandro Bautista-Hernández, Aleksey N. Kolmogorov, and Aldo H. Romero. Structural search for stable Mg-Ca alloys accelerated with a neural network interatomic model. *Physical Chemistry Chemical Physics*, 20(43):27545–27557, 2018.
- [41] E L Kolsbjer, A A Peterson, and B Hammer. Neural-network-enhanced evolutionary algorithm applied to supported metal nanoparticles. *Physical Review B*, 97(19):195424, 2018.
- [42] Albert P. Bartók, James Kermode, Noam Bernstein, and Gábor Csányi. Machine Learning a General-Purpose Interatomic Potential for Silicon. *Physical Review X*, 8(4):41048, 2018.

- [43] Volker L. Deringer, Chris J. Pickard, and Gábor Csányi. Data-Driven Learning of Total and Local Energies in Elemental Boron. *Physical Review Letters*, 120(15):156001, 2018.
- [44] Linfeng Zhang, Jiequn Han, Han Wang, Wissam A. Saidi, Roberto Car, and Weinan E. End-to-end symmetry preserving inter-atomic potential energy model for finite and extended systems, 2018.
- [45] Jonathan Schmidt, Mário R. G. Marques, Silvana Botti, and Miguel A. L. Marques. Recent advances and applications of machine learning in solid-state materials science. *npj Computational Materials*, 5(1):83, 2019.
- [46] Volker L. Deringer, Miguel A. Caro, and Gbor Csnyi. Machine learning interatomic potentials as emerging tools for materials science. *Advanced Materials*, 31(46):1902765, 2019.
- [47] Kyuhyun Lee, Dongsun Yoo, Wonseok Jeong, and Seungwu Han. Simple-nn: An efficient package for training and executing neural-network interatomic potentials. *Computer Physics Communications*, 242:95 – 103, 2019.
- [48] Ruggero Lot, Franco Pellegrini, Yusuf Shaidu, and Emine Kucukbenli. Panna: Properties from artificial neural network architectures, 2019.
- [49] Maximilian Amsler, Samare Rostami, Hossein Tahmasbi, Ehsan Rahmatizad, Somayeh Faraji, Robabe Rasoukhani, and S. Alireza Ghasemi. Flame: a library of atomistic modeling environments, 2019.
- [50] Yunxing Zuo, Chi Chen, Xiangguo Li, Zhi Deng, Yiming Chen, Jrg Behler, Gbor Csnyi, Alexander V. Shapeev, Aidan P. Thompson, Mitchell A. Wood, and Shyue Ping Ong. Performance and cost assessment of machine learning interatomic potentials. *The Journal of Physical Chemistry A*, 124(4):731–745, 2020.
- [51] T. Yokoi, Y. Noda, A. Nakamura, and K. Matsunaga. Neural-network interatomic potential for grain boundary structures and their energetics in silicon. *Phys. Rev. Materials*, 4:014605, Jan 2020.
- [52] Tim Mueller, Alberto Hernandez, and Chuhong Wang. Machine learning for interatomic potential models. *The Journal of Chemical Physics*, 152(5):050902, 2020.
- [53] Andre Lomaka and Toomas Tamm. Linearization of moment tensor potentials for multicomponent systems with a preliminary assessment for short-range interaction energy in water dimer and trimer. *The Journal of Chemical Physics*, 152(16):164115, 2020.
- [54] Xin Chen, Xing-Yu Gao, Ya-Fan Zhao, De-Ye Lin, Wei-Dong Chu, and Hai-Feng Song. Tensoralloy: An automatic atomistic neural network program for alloys. *Computer Physics Communications*, 250:107057, 2020.
- [55] G Kresse and J Hafner. *Ab initio* molecular dynamics for liquid metals. *Physical Review B*, 47(1):558–561, 1993.
- [56] G Kresse and J Furthmüller. Efficient iterative schemes for *ab initio* total-energy calculations using a plane-wave basis set. *Physical Review B*, 54(16):11169–11186, 1996.
- [57] Guillermo Avendao-Franco and Aldo H. Romero. Firefly algorithm for structural search. *Journal of Chemical Theory and Computation*, 12(7):3416–3428, 2016.

[58] Dario Alfè. PHON: A program to calculate phonons using the small displacement method. *Computer Physics Communications*, 180(12):2622–2633, 2009.

[59] Leonardo Dagum and Ramesh Menon. Openmp: An industry-standard api for shared-memory programming. *IEEE Comput. Sci. Eng.*, 5(1):4655, January 1998.

[60] J P Perdew and Alex Zunger. Self-interaction correction to density-functional approximations for many-electron systems. *Physical Review B*, 23(10):5048–5079, 1981.

[61] John P Perdew, Kieron Burke, Matthias Ernzerhof, and Kieron Burke. Generalized gradient approximation made simple. *Physical review letters*, 77(18):3865–3868, 1996.

[62] A. I. Liechtenstein, V. I. Anisimov, and J. Zaanen. Density-functional theory and strong interactions: Orbital ordering in Mott-Hubbard insulators. *Physical Review B*, 52(8):R5467–R5470, 1995.

[63] S L Dudarev, G A Botton, S Y Savrasov, C J Humphreys, and A P Sutton. Electron-energy-loss spectra and the structural stability of nickel oxide: An LSDA+U study. *Physical Review B - Condensed Matter and Materials Physics*, 57(3):1505–1509, 1998.

[64] Jiíí Klimeš, David R Bowler, and Angelos Michaelides. Chemical accuracy for the van der Waals density functional. *Journal of Physics Condensed Matter*, 22(2), 2010.

[65] H Rydberg, M Dion, N Jacobson, E Schröder, P Hyldgaard, S I Simak, D C Langreth, and B I Lundqvist. Van der waals density functional for layered structures. *Physical Review Letters*, 91(12):126402, 2003.

[66] Jianwei Sun, Adrienn Ruzsinszky, and John P. Perdew. Strongly constrained and appropriately normed semilocal density functional. *Phys. Rev. Lett.*, 115:036402, Jul 2015.

[67] D M Daven, N Tit, J R Morris, and K M Ho. Structural optimization of Lennard-Jones clusters by a genetic algorithm. *Chemical Physics Letters*, 256(1-2):195–200, 1996.

[68] C Barrón, S Gómez, D Romero, and A Saavedra. A genetic algorithm for Lennard-Jones atomic clusters. *Applied Mathematics Letters*, 12(7):85–90, 1999.

[69] Xueguang Shao, Longjiu Cheng, and Wensheng Cai. A dynamic lattice searching method for fast optimization of Lennard-Jones clusters. *Journal of Computational Chemistry*, 25(14):1693–1698, 2004.

[70] Xueguang Shao, Xiaoli Yang, and Wensheng Cai. A dynamic lattice searching method with interior operation for unbiased optimization of large Lennard-Jones clusters. *Journal of Computational Chemistry*, 29(11):1772–1779, 2008.

[71] Xia Wu, Wensheng Cai, and Xueguang Shao. A dynamic lattice searching method with rotation operation for optimization of large clusters. *Chemical Physics*, 363(1-3):72–77, 2009.

[72] Stefan Goedecker. Minima hopping: An efficient search method for the global minimum of the potential energy surface of complex molecular systems Communication. *The Journal of Chemical Physics*, 120(121):114105–144102, 2004.

[73] Chris J. Pickard and R. J. Needs. *Ab initio* random structure searching. *Journal of Physics Condensed Matter*, 23(5):53201, 2011.

[74] David J Wales and Jonathan P K Doye. Global optimization by basin-hopping and the lowest energy structures of Lennard-Jones clusters containing up to 110 atoms. *Journal of Physical Chemistry A*, 101(28):5111–5116, 1997.

[75] Hyoung Gyu Kim, Si Kyung Choi, and Hyuck Mo Lee. New algorithm in the basin hopping Monte Carlo to find the global minimum structure of unary and binary metallic nanoclusters. *Journal of Chemical Physics*, 128(14):144702, 2008.

[76] David J Wales and Harold A Scheraga. Global optimization of clusters, crystals, and biomolecules. *Science*, 285(5432):1368–1372, 1999.

[77] Seth T Call, Dmitry Yu Zubarev, and Alexander I Boldyrev. Global minimum structure searches via particle swarm optimization. *Journal of Computational Chemistry*, 28(7):1177–1186, 2007.

[78] Jian Lv, Yanchao Wang, Li Zhu, and Yanming Ma. Particle-swarm structure prediction on clusters. *Journal of Chemical Physics*, 137(8):84104, 2012.

[79] Xia Wu and Yan Sun. Stable structures and potential energy surface of the metallic clusters: Ni, Cu, Ag, Au, Pd, and Pt. *Journal of Nanoparticle Research*, 19(6):201, 2017.

[80] A. F. Bialon, T. Hammerschmidt, R. Drautz, S. Shah, E. R. Margine, and A. N. Kolmogorov. Possible routes for synthesis of new boron-rich Fe-B and $Fe_{1-x}Cr_xB_4$ compounds. *Applied Physics Letters*, 98(8):81901, 2011.

[81] Huiyang Gou, Natalia Dubrovinskaia, Elena Bykova, Alexander A. Tsirlin, Deepa Kasinathan, Walter Schnelle, Asta Richter, Marco Merlini, Michael Hanfland, Artem M. Abakumov, Dmitry Batuk, Gustaaf Van Tendeloo, Yoichi Nakajima, Aleksey N. Kolmogorov, and Leonid Dubrovinsky. Discovery of a superhard iron tetraboride superconductor. *Phys. Rev. Lett.*, 111:157002, Oct 2013.

[82] Aleksey N. Kolmogorov and Stefano Curtarolo. Prediction of different crystal structure phases in metal borides: A lithium monoboride analog to MgB_2 . *Physical Review B - Condensed Matter and Materials Physics*, 73(18):180501, 2006.

[83] Aleksey N Kolmogorov and Stefano Curtarolo. Theoretical study of metal borides stability. *Physical Review B - Condensed Matter and Materials Physics*, 74(22):224507, 2006.

[84] A. N. Kolmogorov, S. Hajinazar, C. Angyal, V. L. Kuznetsov, and A. P. Jephcoat. Synthesis of a predicted layered LiB via cold compression. *Physical Review B - Condensed Matter and Materials Physics*, 92(14):144110, 2015.

[85] Junping Shao, Clément Beaufils, and Aleksey N. Kolmogorov. *Ab initio* engineering of materials with stacked hexagonal tin frameworks. *Scientific Reports*, 6:28369, 2016.

[86] Joshua M. Stratford, Martin Mayo, Phoebe K. Allan, Oliver Pecher, Olaf J. Borkiewicz, Kamila M. Wiaderek, Karena W. Chapman, Chris J. Pickard, Andrew J. Morris, and Clare P. Grey. Investigating sodium storage mechanisms in tin anodes: A combined pair distribution function analysis, density functional theory, and solid-state nmr approach. *Journal of the American Chemical Society*, 139(21):7273–7286, 2017.

[87] F. Sun, H. Zheng, Y. Liu, E. D. Sandoval, C. Xu, J. Xu, C. Q. Jin, C. J. Sun, W. G. Yang, H. K. Mao, J. F. Mitchell, A. N. Kolmogorov, and D. Haskel. Electronic and structural response to pressure in the hyperkagome-lattice $\text{Na}_3\text{Ir}_3\text{O}_8$. *Physical Review B*, 98(8):85131, 2018.

[88] S. K. Choi, R. Coldea, A. N. Kolmogorov, T. Lancaster, I. I. Mazin, S. J. Blundell, P. G. Radaelli, Yogesh Singh, P. Gegenwart, K. R. Choi, S.-W. Cheong, P. J. Baker, C. Stock, and J. Taylor. Spin waves and revised crystal structure of honeycomb iridate Na_2IrO_3 . *Phys. Rev. Lett.*, 108:127204, Mar 2012.

[89] Haiyang Niu, Jiaqi Wang, Xing-Qiu Chen, Dianzhong Li, Yiyi Li, Petr Lazar, Raimund Podloucky, and Aleksey N. Kolmogorov. Structure, bonding, and possible superhardness of crb_4 . *Phys. Rev. B*, 85:144116, Apr 2012.

[90] A G Van Der Geest and A N Kolmogorov. Stability of 41 metal-boron systems at 0 GPa and 30 GPa from first principles. *Calphad: Computer Coupling of Phase Diagrams and Thermochemistry*, 46:184–204, 2014.

[91] Arno Knapschneider, Christian Litterscheid, Nathan C. George, Jakoah Brgoch, Norbert Wagner, Johannes Beck, Joshua A. Kurzman, Ram Seshadri, and Barbara Albert. Peierls-distorted monoclinic mnb_4 with a mnmn bond. *Angewandte Chemie International Edition*, 53(6):1684–1688, 2014.

[92] Haiyang Niu, Xing-Qiu Chen, Weijun Ren, Qiang Zhu, Artem R. Oganov, Dianzhong Li, and Yiyi Li. Variable-composition structural optimization and experimental verification of mnb_3 and mnb_4 . *Phys. Chem. Chem. Phys.*, 16:15866–15873, 2014.

[93] Is orthorhombic iron tetraboride superhard? *Journal of Materomics*, 1(1):45 – 51, 2015.

[94] J. Bekaert, A. Aperis, B. Partoens, P. M. Oppeneer, and M. V. Milošević. Advanced first-principles theory of superconductivity including both lattice vibrations and spin fluctuations: The case of feb_4 . *Phys. Rev. B*, 97:014503, Jan 2018.

[95] Jun Nagamatsu, Norimasa Nakagawa, Takahiro Muranaka, Yuji Zenitani, and Jun Akimitsu. Superconductivity at 39 K in magnesium diboride. *Nature*, 410(6824):63–64, 2001.

[96] Yogesh Singh and P. Gegenwart. Antiferromagnetic mott insulating state in single crystals of the honeycomb lattice material Na_2IrO_3 . *Phys. Rev. B*, 82:064412, Aug 2010.

[97] Arno Knapschneider, Christian Litterscheid, Dmytro Dzivenko, Joshua A. Kurzman, Ram Seshadri, Norbert Wagner, Johannes Beck, Ralf Riedel, and Barbara Albert. Possible superhardness of crb_4 . *Inorganic Chemistry*, 52(2):540–542, 2013.

[98] <https://github.com/maise-guide/maise>.

[99] <https://github.com/maise-guide/maise-net>.

[100] Mark Galassi and Brian Gough. *GNU Scientific Library Reference Manual (3rd Ed.)*. Network Theory Ltd., 3 edition, 2001.

[101]

[102] Siva Chiriki, Shweta Jindal, and Satya S Bulusu. Neural network potentials for dynamics and thermodynamics of gold nanoparticles. *Journal of Chemical Physics*, 146(8):84314, 2017.

- [103] H. Bernhard Schlegel. Optimization of equilibrium geometries and transition structures. *Journal of Computational Chemistry*, 3(2):214–218, 1982.
- [104] Magnus R Hestenes and Eduard Stiefel. Methods of conjugate gradients for solving linear systems. *Journal of Research of the National Bureau of Standards*, 49(6):2379, 1952.
- [105] Loup Verlet. Computer "experiments" on classical fluids. i. thermodynamical properties of lennard-jones molecules. *Phys. Rev.*, 159:98–103, Jul 1967.
- [106] Shuichi Nose. A unified formulation of the constant temperature molecular dynamics methods. *The Journal of Chemical Physics*, 81(1):511–519, 1984.
- [107] William G. Hoover. Canonical dynamics: Equilibrium phase-space distributions. *Phys. Rev. A*, 31:1695–1697, Mar 1985.
- [108] H. J. C. Berendsen, J. P. M. Postma, W. F. van Gunsteren, A. DiNola, and J. R. Haak. Molecular dynamics with coupling to an external bath. *The Journal of Chemical Physics*, 81(8):3684–3690, 1984.
- [109] Dwight E. Gray. *American Institute of Physics (AIP). Handbook*. 1972.
- [110] Qiang Zhu, Artem R. Oganov, and Andriy O. Lyakhov. Evolutionary metadynamics: a novel method to predict crystal structures. *CrystEngComm*, 14:3596–3601, 2012.
- [111] Ernesto D. Sandoval, Samad Hajinazar, and Aleksey N. Kolmogorov. Stability of two-dimensional BN-Si structures. *Physical Review B*, 94(9):94105, 2016.
- [112] Artem R. Oganov and Mario Valle. How to quantify energy landscapes of solids. *Journal of Chemical Physics*, 130(10):104504, 2009.
- [113] Raju P Gupta. Lattice relaxation at a metal surface. *Physical Review B*, 23(12):6265–6270, 1981.
- [114] A P Sutton and J Chen. Long-range finnis-sinclair potentials. *Philosophical Magazine Letters*, 61(3):139–146, 1990.
- [115] J. E. Jones. On the Determination of Molecular Fields. II. From the Equation of State of a Gas. *Proceedings of the Royal Society A: Mathematical, Physical and Engineering Sciences*, 106(738):463–477, 1924.
- [116] J Tersoff. New empirical model for the structural properties of silicon. *Physical Review Letters*, 56(6):632–635, 1986.
- [117] Murray S Daw and M I Baskes. Semiempirical, quantum mechanical calculation of hydrogen embrittlement in metals. *Physical Review Letters*, 50(17):1285–1288, 1983.
- [118] M Wilson and P A Madden. Polarization effects in ionic systems from first principles. *Journal of Physics: Condensed Matter*, 5(17):2687–2706, 1993.
- [119] Aleksey N Kolmogorov and Vincent H Crespi. Registry-dependent interlayer potential for graphitic systems. *Physical Review B - Condensed Matter and Materials Physics*, 71(23):235415, 2005.

[120] Adri C. T. van Duin, Siddharth Dasgupta, Francois Lorant, and William A. Goddard. Reaxff: A reactive force field for hydrocarbons. *The Journal of Physical Chemistry A*, 105(41):9396–9409, 2001.

[121] M. W. Finnis and J. E. Sinclair. A simple empirical n-body potential for transition metals. *Philosophical Magazine A*, 50(1):45–55, 1984.

[122] D. G. Pettifor and I. I. Oleinik. Analytic bond-order potentials beyond tersoff-brenner. i. theory. *Phys. Rev. B*, 59:8487–8499, Apr 1999.

[123] Volker L. Deringer, Davide M. Proserpio, Gbor Csnyi, and Chris J. Pickard. Data-driven learning and prediction of inorganic crystal structures. *Faraday Discuss.*, 211:45–59, 2018.

[124] Noam Bernstein, Gábor Csányi, and Volker L. Deringer. De novo exploration and self-guided learning of potential-energy surfaces. *npj Computational Materials*, 5(1):99, Oct 2019.

[125] Evgeny V. Podryabinkin and Alexander V. Shapeev. Active learning of linearly parametrized interatomic potentials. *Computational Materials Science*, 140:171 – 180, 2017.

[126] Evgeny V. Podryabinkin, Evgeny V. Tikhonov, Alexander V. Shapeev, and Artem R. Oganov. Accelerating crystal structure prediction by machine-learning interatomic potentials with active learning. *Phys. Rev. B*, 99:064114, Feb 2019.

[127] Luigi Bonati and Michele Parrinello. Silicon liquid structure and crystal nucleation from ab initio deep metadynamics. *Phys. Rev. Lett.*, 121:265701, Dec 2018.

[128] A.N. Kolmogorov. *Study of Bonding and Doping Properties of sp^2 Carbon Nanostructures: Numerical Simulations and Development of Empirical Interaction Potentials*. The Pennsylvania State University, 2004.

[129] Atsuto Seko, Yukinori Koyama, and Isao Tanaka. Cluster expansion method for multicomponent systems based on optimal selection of structures for density-functional theory calculations. *Physical Review B - Condensed Matter and Materials Physics*, 80(16):165122, 2009.

[130] S. Núñez and R. L. Johnston. Structures and chemical ordering of small Cu-Ag clusters. *Journal of Physical Chemistry C*, 114(31):13255–13266, 2010.

[131] A Urban, M Reese, M Mrovec, C Elsässer, and B Meyer. Parameterization of tight-binding models from density functional theory calculations. *Physical Review B - Condensed Matter and Materials Physics*, 84(15):155119, 2011.

[132] Albert P. Bartók, Risi Kondor, and Gábor Csányi. On representing chemical environments. *Physical Review B - Condensed Matter and Materials Physics*, 87(18):184115, 2013.

[133] Sergey N. Pozdnyakov, Michael J. Willatt, Albert P. Bartk, Christoph Ortner, Gbor Csnyi, and Michele Ceriotti. On the completeness of atomic structure representations, 2020.

[134] Andrei A. Rusu, Neil C. Rabinowitz, Guillaume Desjardins, Hubert Soyer, James Kirkpatrick, Koray Kavukcuoglu, Razvan Pascanu, and Raia Hadsell. Progressive neural networks, 2016.

[135] Jaehong Yoon, Eunho Yang, Jeongtae Lee, and Sung Ju Hwang. Lifelong learning with dynamically expandable networks, 2017.

[136] Berk Onat, Ekin D Cubuk, Brad D Malone, and Efthimios Kaxiras. Implanted neural network potentials: Application to Li-Si alloys. *Physical Review B*, 97(9):94106, 2018.

[137] Sönke Lorenz, Matthias Scheffler, and Axel Gross. Descriptions of surface chemical reactions using a neural network representation of the potential-energy surface. *Physical Review B - Condensed Matter and Materials Physics*, 73(11):115431, 2006.

[138] Albert P Bartók, Michael J Gillan, Frederick R Manby, and Gábor Csányi. Machine-learning approach for one- and two-body corrections to density functional theory: Applications to molecular and condensed water. *Physical Review B - Condensed Matter and Materials Physics*, 88(5):54104, 2013.

[139] G A Tribello, M Ceriotti, and M Parrinello. Using sketch-map coordinates to analyze and bias molecular dynamics simulations. *Proceedings of the National Academy of Sciences*, 109(14):5196–5201, 2012.

[140] Anthony M Reilly, Derek S Middlemiss, M Murshed Siddick, Derek A Wann, Graeme J Ackland, Chick C Wilson, David W H Rankin, and Carole A Morrison. The phonon spectrum of phase-I ammonia: reassignment of lattice mode symmetries from combined molecular and lattice dynamics calculations. *Journal of Physical Chemistry A*, 112(6):1322–1329, 2008.

[141] Diogo A R S Latino, Filomena F M Freitas, João Aires-De-Sousa, and Fernando M.S.Silva Fernandes. Neural networks to approach potential energy surfaces: Application to a molecular dynamics simulation. *International Journal of Quantum Chemistry*, 107(11):2120–2132, 2007.

[142] J. S. Smith, O. Isayev, and A. E. Roitberg. Ani-1: an extensible neural network potential with dft accuracy at force field computational cost. *Chem. Sci.*, 8:3192–3203, 2017.

[143] Mariia Karabin and Danny Perez. An entropy-maximization approach to automated training set generation for interatomic potentials, 2020.

[144] Linfeng Zhang, De-Ye Lin, Han Wang, Roberto Car, and Weinan E. Active learning of uniformly accurate interatomic potentials for materials simulation. *Phys. Rev. Materials*, 3:023804, Feb 2019.

[145] Pavel E. Dolgirev, Ivan A. Kruglov, and Artem R. Oganov. Machine learning scheme for fast extraction of chemically interpretable interatomic potentials. *AIP Advances*, 6(8):085318, 2016.

[146] Andrew A Peterson. Acceleration of saddle-point searches with machine learning. *Journal of Chemical Physics*, 145(7):74106, 2016.

[147] Si Da Huang, Cheng Shang, Xiao Jie Zhang, and Zhi Pan Liu. Material discovery by combining stochastic surface walking global optimization with a neural network. *Chemical Science*, 8(9):6327–6337, 2017.

[148] Zachary W Ulissi, Michael T Tang, Jianping Xiao, Xinyan Liu, Daniel A Torelli, Mohammadreza Karamad, Kyle Cummins, Christopher Hahn, Nathan S Lewis, Thomas F Jaramillo, Karen Chan, and Jens K Nørskov. Machine-learning methods enable exhaustive searches for active Bimetallic facets and reveal active site motifs for CO₂ reduction. *ACS Catalysis*, 7(10):6600–6608, 2017.

[149] J. Towns, T. Cockerill, M. Dahan, I. Foster, K. Gaither, A. Grimshaw, V. Hazlewood, S. Lathrop, D. Lifka, G. D. Peterson, R. Roskies, J. R. Scott, and N. Wilkins-Diehr. Xsede: Accelerating scientific discovery. *Computing in Science Engineering*, 16(5):62–74, 2014.